

Review

Investigation of Hydrogen Production System-Based PEM EL: PEM EL Modeling, DC/DC Power Converter, and Controller Design Approaches

Mohamed Koundi ^{1,*}, Hassan El Fadil ¹, Zakaria EL Idrissi ¹, Abdellah Lassioui ¹, Abdessamad Intidam ¹, Tasnime Bouanou ¹, Soukaina Nady ¹ and Aziz Rachid ^{1,2}

¹ ASE Laboratory, National School of Applied Sciences (ENSA), Ibn Tofail University, Kénitra 14000, Morocco

² LSIB Laboratory, FST, Hassan II University of Casablanca, Mohammedia 28806, Morocco

* Correspondence: mohamed.koundi.mk@gmail.com

Abstract: The main component of the hydrogen production system is the electrolyzer (EL), which is used to convert electrical energy and water into hydrogen and oxygen. The power converter supplies the EL, and the controller is used to ensure the global stability and safety of the overall system. This review aims to investigate and analyze each one of these components: Proton Exchange Membrane Electrolyzer (PEM EL) electrical modeling, DC/DC power converters, and control approaches. To achieve this desired result, a review of the literature survey and an investigation of the PEM EL electrical modeling of the empirical and semi-empirical, including the static and dynamic models, are carried out. In addition, other sub-models used to predict the temperature, gas flow rates (H₂ and O₂), hydrogen pressure, and energy efficiency for PEM EL are covered. DC/DC power converters suitable for PEM EL are discussed in terms of efficiency, current ripple, voltage ratio, and their ability to operate in the case of power switch failure. This review involves analysis and investigation of PEM EL control strategies and approaches previously used to achieve control objectives, robustness, and reliability in studying the DC/DC converter-PEM electrolyzer system. The paper also highlights the online parameter identification of the PEM electrolyzer model and adaptive control issues. Finally, a discussion of the results is developed to emphasize the strengths, weaknesses, and imperfections of the literature on this subject as well as proposing ideas and challenges for future work.

Keywords: hydrogen; PEM electrolyzer; DC/DC converter; equivalent electrical model; control strategies; parameter identification



Citation: Koundi, M.; El Fadil, H.; EL Idrissi, Z.; Lassioui, A.; Intidam, A.; Bouanou, T.; Nady, S.; Rachid, A. Investigation of Hydrogen Production System-Based PEM EL: PEM EL Modeling, DC/DC Power Converter, and Controller Design Approaches. *Clean Technol.* **2023**, *5*, 531–568. <https://doi.org/10.3390/cleantechnol5020028>

Academic Editor: Damien Guilbert

Received: 3 January 2023

Revised: 8 March 2023

Accepted: 10 April 2023

Published: 23 April 2023



Copyright: © 2023 by the authors. Licensee MDPI, Basel, Switzerland. This article is an open access article distributed under the terms and conditions of the Creative Commons Attribution (CC BY) license (<https://creativecommons.org/licenses/by/4.0/>).

1. Introduction

Due to greenhouse gas emissions, the climatic crises have become a salient issue that interests the whole world. In the last decade, many efforts have been carried out to fight climatic change, such as the Intergovernmental Panel on Climate Change (IPCC), which has served to study and understand climate change and its effects on our planet. Additionally, many countries signed the international treaty of the Kyoto Protocol which is aimed to reduce greenhouse gas emissions. The current global crisis of the COVID-19 pandemic gave us essential lessons on dealing with global issues such as climatic crises before they are hard to control. We learned from this crisis that it is high time to make efforts, strengthen solidarity among countries, and educate them regarding delaying dealing with crises as that will have repercussions that will indeed threaten the whole of humanity [1,2].

To try to solve this climatic crisis we face today and limit greenhouse gas emissions, we must reduce fossil fuel energy by integrating renewable energy sources (RES). For example, photovoltaic (PV) panels, and wind turbines (WT) are the most widely used intermittent RES. Unfortunately, these sources have a volatile behavior that complicates electrical energy management [3]. The basic solution to this issue is to add efficient electrical energy storage systems. The storage of electrical energy produced by RES in the shape of

hydrogen is one of the most efficient, clean, and promising energy vectors [4]. The water electrolyzers are the elements usually used to convert electrical energy into pure hydrogen. The hydrogen produced can be stored in hydrogen tanks so that it can be restored by fuel cells into electrical energy, which gives a degree of freedom to the electrical power generation consisting of intermittent RES.

The PEM EL and alkaline electrolyzer, which produce pure hydrogen, have been studied extensively by researchers in the last decade. PEM ELs have many advantages over the alkaline electrolyzers, including their ability to operate at high current density, which makes them more compact, and their higher efficiency and ability to produce hydrogen at high pressure. They also have a fast-dynamic response, high purity of hydrogen, and the best safety degree [5–7]. However, PEM ELs require expensive catalysts, typically platinum and iridium, which increases their manufacturing cost. In recent years, researchers have been working to reduce the cost of PEM ELs by developing new catalyst materials or reducing the use of noble catalysts, in order to make PEM ELs commercially available [8–12].

The PEM EL modeling by an Equivalent Electrical Circuit (EEC) is the best way to predict the PEM EL behavior and diagnose its lifetime, analyzing performances and its uses in simulating, monitoring, and optimizing operation and energy efficiency. The EEC is a powerful tool for identifying parameters [6,13–15].

PEM EL cannot be powered directly from RES. It usually requires electronic power converters interfacing among the PEM EL, DC bus, and AC grid. DC/DC converters are essentially the most widely used converters to supply the PEM EL from RES. Choosing the most appropriate DC/DC converter is a crucial step to conversion ratio, current ripple, and operating ability in case of power switch failure [16–19].

Elaboration of the control strategies for the DC/DC converter is necessary to ensure the stability of the PEM EL-DC/DC converter system, optimize the energy efficiency, manage hydrogen flow rate, and regulate the operation point of PEM EL [19–22]. PEM EL models contain many parameters that are very sensitive to operating conditions. Online parameter identification and adaptive control approach remain powerful tools for robust control to solve this problem.

Recently, several reviews have been reported in the literature about PEM EL modeling. Reference [23] has presented a short survey of the empirical, semi-empirical, analytical, and mechanical models. This review focused on the mass transport in the PEM EL cells (water transport and gas cross-over). Reference [24] has comprehensively analyzed different modeling approaches for low-temperature PEM EL and alkaline electrolyzer, including the thermal and fluid sub-models. Reference [25] has presented the static and dynamic PEM EL models for the electrical domain modeling and has compared the static and dynamic models. Additionally, PEM EL analyzed energy efficiency and specific energy consumption. In reference [26], a review has discussed superficial modeling to describe the cell voltage of PEM EL based on the empirical and analytical models, presented the different dynamic models, and discussed the two-phase flow issue in the PEM EL cell. In reference [27], a comparison of multiple DC/DC converters has been used to supply the PEM EL in terms of current ripple, energy efficiency, voltage ratio, electromagnetic interference, cost, and continuity of service in the case of power switch failures. Reference [28] discussed the DC/DC converter suitable with PEM EL models for power converter control. Moreover, a comparison between the static and dynamic PEM EL has developed. In reference [18], the authors investigated the AC/DC converter interfacing between the PEM EL and alternative sources. There is a recent study presented in [29] where a graphical platform was developed to make it easier for users to interact and understand the simulation results of PEM electrolyzer systems. This platform also allows users to evaluate and simulate the performance of PEM electrolyzer models under different conditions in a more efficient and accurate way, leading to a better understanding of these systems and improving their design and optimization.

As mentioned above, we examined several reviews of work on the PEM EL modeling and others on the DC/DC converters appropriate to PEM EL. Recently, a few surveys

have worked on the control system suitable with DC/DC converter-PEM EL. Contrary to fuel cells, the PEM EL online parameter identification issues are not well discussed in the literature, despite their importance in obtaining an accurate model and robust control. No review investigates and analyzes the interaction between the electrical modeling of PEM EL models for DC/DC converter and the control system.

The main contribution of this review is to investigate and analyze each sub-system, i.e., the PEM EL model, DC/DC converter, and control system, as follows:

- Investigate and analyze the PEM EL models concerning transforming these models into the equivalent electrical circuit because it is more convenient with power converters and controller design. On the other hand, it evaluates the different models describing the dynamic behavior, the number of parameters, complexity, accuracy range, and suitability with a control problem.
- Investigate the interaction between the DC/DC converters and PEM EL in terms of current ripple, energy efficiency, voltage ratio, electromagnetic interference, cost, and continuity of service in the case of power switch failures.
- Analyze and summarize the linear and nonlinear control strategies by considering the interaction between the PEM EL and DC/DC converter systems regarding their validity, reliability, and controller robustness under parameter variations.

2. Presentation of the Hydrogen Production System Based on PEM EL Technology

As shown in Figure 1, the hydrogen production system based on the PEM EL transforms the electrical energy from the DC bus and water into hydrogen, oxygen, and heat. The second element of the DC/DC converter serves to interface the PEM EL with the DC bus, and, finally, the controller aims to control the current or voltage of PEM EL to optimize energy efficiency, hydrogen flow rate management, and other operations. Other subsystems should be added as a thermal management system to control the PEM EL temperature, and a gas pressure regulator should be used to govern the pressure in the gas separators for testing or operating reasons, among other things.

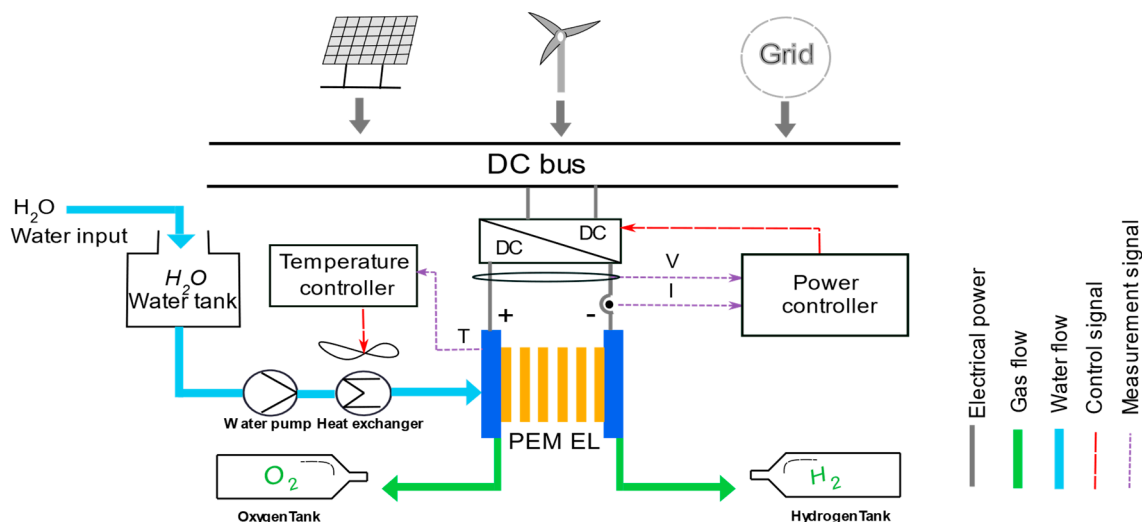
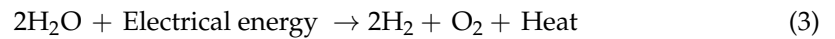
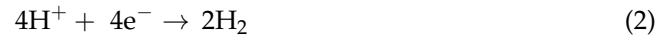


Figure 1. Hydrogen production system based on the PEM EL.

The PEM EL technology is similar to PEM fuel cell technology. In the anode catalyst layer, under the influence of an electrical field, two water molecules split into four protons and oxygen molecules. The oxygen exits the anode electrode and travels to the anode flow field through the anode gas diffusion layer. Meanwhile, the protons travel through the proton exchange membrane and reach the cathode catalyst layer, where they combine with electrons from the external circuit to form hydrogen. The hydrogen leaves the cathode to the cathode flow field through the cathode gas diffusion layer [30–32]. The electrochemical

reactions at the anode, the cathode, and the overall reaction are expressed by the following equations respectively:



3. Electrical Modeling of PEM

The electrical modeling of PEM EL is a salient and powerful tool used to describe the electrical characteristic (i.e., the relationship between the applied voltage and current density of PEM EL). The electrical modeling of the PEM EL can be modeled by equivalent electrical circuits that facilitate the modeling of PEM EL, including power electronic converters that can be used for simulation, diagnosis, identification issues, and controller design. Several types of electrical modeling of PEM EL have developed relying on the empirical and semi-empirical approaches; most of these models describe the electrical characteristic at steady-state operation, and a few models consider the dynamic behavior. Figure 2 illustrates the classification of the electrical models.

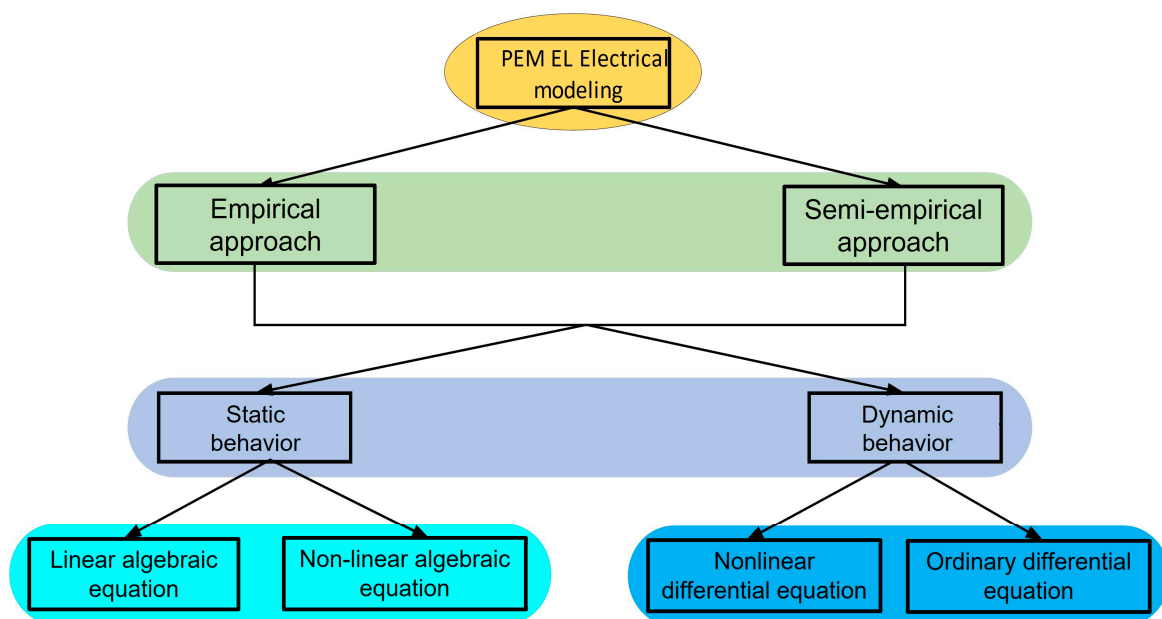


Figure 2. Classification of PEM EL electrical modeling.

3.1. Empirical Approach

The electrical characteristic of PEM EL can be described by an empirical approach using the empirical equations and experimental data to obtain the parameters, except that the models have a physical meaning (ohmic resistance, voltage, activation, etc.) which we will discuss in this work because it is possible to transform them into EEC.

3.1.1. Static Modeling

Most of the PEM EL electrical models based on the empirical approach are static models which describe the electrical characteristic at steady-state operation, known as the polarization curve.

Among the simplest static models in the literature suggested by Atlam et al. [33] and reported by several works [30,34–36], this model fits perfectly between the polarization curve of the PEM EL model and the measurement data. It can also predict the hydrogen production rate with a relative error of less than 2%. This model is expressed by algebraic linear

equation. Equation (4) consists of an ohmic resistance R_{ohm} and a reversible voltage E_{rev} as a function of pressure and temperature that are expressed by Equations (5) and (6) [34]:

$$V_{el} = R_{ohm}(\theta, p) \times I_{el} + E_{rev}(\theta, p) \tag{4}$$

$$R_{ohm}(\theta, p) = R_0 + k \times \ln\left(\frac{p}{p_0}\right) + dR_\theta(\theta - \theta_0) \tag{5}$$

$$E_{rev}(\theta, p) = E_{rev}^0 + \frac{R(273.15 + \theta)}{2F} \ln\left(\frac{p}{p_0}\right) \tag{6}$$

where R_0 , p_0 , and θ_0 are ohmic resistance, pressure, and temperature at reference conditions. k is a constant parameter fitting, and dR_θ (Ohm/ C^0) is an ohmic resistance coefficient of temperature. The E_{rev}^0 is a reversible voltage at reference conditions. Additionally, this model introduced the ideal voltage V_i as an essential term for calculating the useful power P_{H_2} (Equation (7)) and the efficiency of the PEM EL (Equation (8)). Finally, the EEC shown in Figure 3 can be designed in Equation (4)–(7):

$$P_{H_2} = V_i I_{el} \tag{7}$$

$$\eta_{el} = \frac{P_{H_2}}{P} = \frac{V_i I_{el}}{V_{el} I_{el}} = \frac{V_i}{V_{el}} \tag{8}$$

where P is absorbed electrical power by PEM EL.

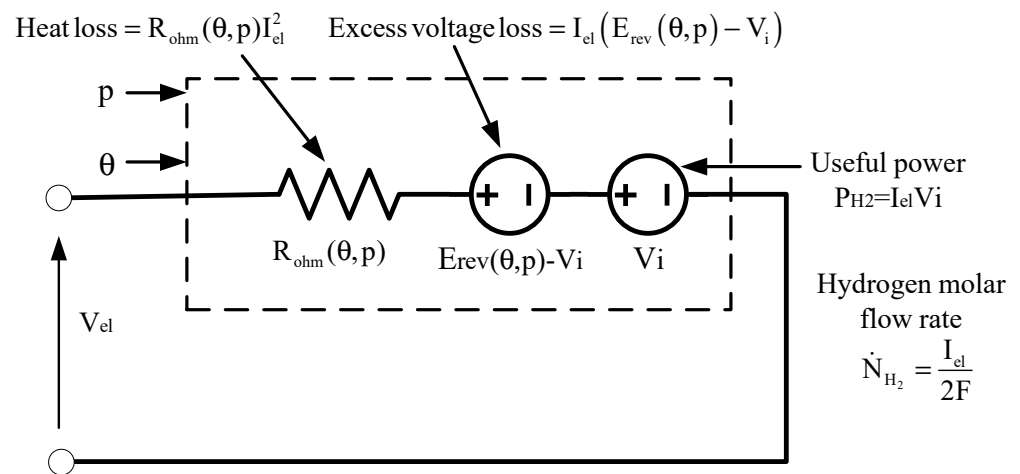


Figure 3. Atlam PEM EL equivalent electrical circuit [34].

Additionally, Ullberg [37] developed a static model described by a nonlinear algebraic equation (Equation (9)) for an alkaline electrolyzer which took into account the effect of temperature and pressure [37–40], and some authors used it for PEM EL by changing the fitting parameters [41,42].

The first term presents the reversible voltage determined from the Nernst equation and fundamental thermodynamics laws. The parameters s_1 , s_2 , s_3 , r_1 , r_2 , t_1 , t_2 , and t_3 were obtained using one of the identification methods. The calculation details can be found in the semi-empirical model’s section or see reference [42].

This empirical model can be transformed in EEC using ohmic resistance to represent the second term and two voltage sources: the first for reversible voltage and the second for the logarithmic term, as illustrated in Figure 4.

$$V_{el} = E_{rev}(\theta, p) + \frac{(r_1 + r_2 \theta)}{A} I_{el} + (s_1 + s_2 \theta + s_3 \theta^2) \log\left(\frac{t_1 + \frac{t_2}{\theta} + \frac{t_3}{\theta^2} I_{el} + 1}{A}\right) \tag{9}$$

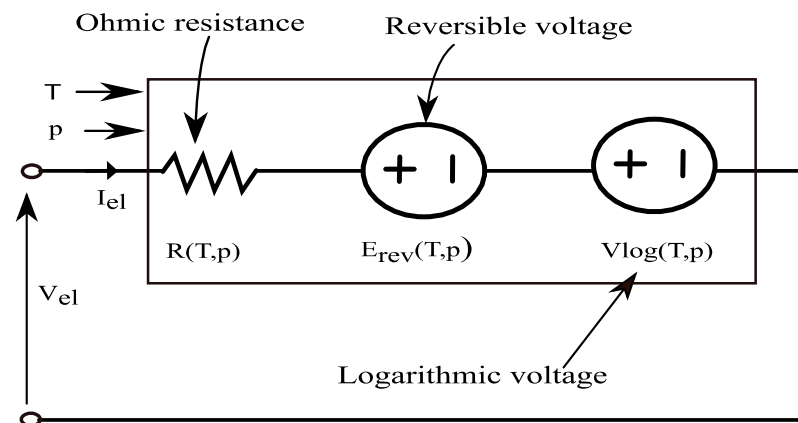


Figure 4. Ulleberg PEM EL equivalent electrical circuit.

3.1.2. Dynamic Modeling

Dynamic modeling makes it possible to describe the actual behavior of the PEM EL in a more precise and reliable manner, particularly when the PEM EL is coupled to intermittent RES and when the operating conditions change fast over time [43]. Like fuel cells, several dynamic empirical models have been developed in the literature using electrochemical impedance spectroscopy (EIS) and the current interruption technique (IC).

Electrochemical Impedance Spectroscopy

Electrochemical impedance spectroscopy (EIS) is a salient technique used in several areas. The application of this technique has countless contributions as degradation analysis and as diagnostic tools of the water electrolyzer [44–48]. However, only one study exploits this technique to provide a dynamic model of PEM EL powered by PV with a DC/DC buck converter to regulate the hydrogen flow rate [49].

The principle of the EIS technique consists of applying on the PEM EL a sinusoidal current in a frequency range of 1mHz to 100KHz to the direct current; as shown in Figure 5, the amplitude of the current should be small to linearize the behavior of the PEM EL around the operating point [50]; the experimental data of EIS presented in the Nyquist plot to model the complex impedance of PEM EL.

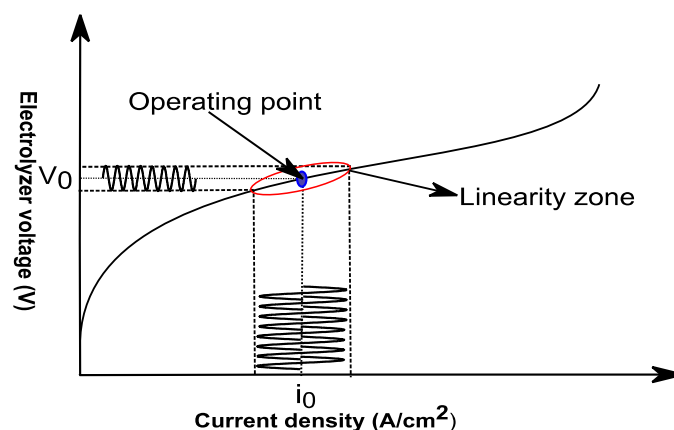


Figure 5. Schematic representation of EIS applied to PEM EL.

In literature, several EECs are discussed in references [51,52]. Generally, the Randles circuit (Figure 6) and Randles–Warburg circuit (Figure 7) are suitable for the electronic converter [48,49,53–55]. The Warburg circuit includes all electrochemical processes: ohmic resistance (R_{ohm}), activation losses, double-layer capacity (C_{dl}), and concentration losses (Z_{wbg}). However, the Randles circuit neglects the concentration losses that make the EEC have a deviation, especially at high current density. This model predicts the behavior of

PEM EL at the current operating density when the contribution of concentration losses is ultralow.

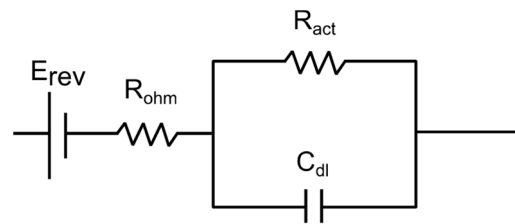


Figure 6. Randles circuit.

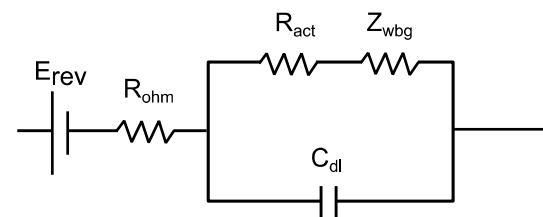


Figure 7. Randles-Warburg circuit.

After dozens of experimental data, the parameters of the electrical equivalent are calculated using the Nyquist plot, then the optimal parameters are obtained by the identification algorithm, which minimizes the difference between calculation and measurement value [52].

The advantage of using the EIS technique to model the PEM EL is that this technique describes the different electrochemical processes, including dynamic behavior [51], and we can present them in the form of an electrical circuit, which is suitable with electronic converters. However, the major disadvantage of the EIS technique is that it requires a high cost of equipment, but recently, this problem has been overcome in some applications using only the DC-DC converter and exploiting the controller element to use the EIS technique. For more details, see [48]. The electrochemical processes cannot be presented by pure electrical components (resistance, capacitor, inductance). Periodically, we use a constant phase element instead of the capacitor when we have a surface irregularity or a non-uniform current distribution [51]. In addition, the equivalent electrical model is validated only in the neighborhood of the operating point (tested point) [52], which limits the use of the equivalent model in a wide operation range.

Current Interruption

The Current Interruption CI technique has the same objective as EIS and is used to derive the parameters of EEC. In the literature, only [50,53,56] have tackled this technique to model the PEM EL in the EEC form. These studies have suggested two methods based on the CI technique: the nature voltage response method (NVR) and system identification (SI). The first method is suitable for Randles circuit when the concentration losses are neglected [53]. In this case, in a steady state and at the operating point, the electric current through PEM EL interrupts instantaneously. From the NVR, we can determine the parameters of Randles' circuit as shown in Figure 8, the drop voltage between V_0 and V_1 caused by ohmic resistance of the PEM EL, the exponential decay from V_1 to V_2 due to discharge of the capacitor through the charge transfer resistance, and therefore, the three parameters are calculated as follows [50]:

$$R_{\text{ohm}} = \frac{V_0 - V_1}{I_0} \quad (10)$$

$$R_{\text{act}} = \frac{V_1 - V_2}{I_0} \quad (11)$$

$$C_{dl} = \frac{\tau_{dl}}{R_{act}} \quad (12)$$

where the τ_{dl} is the time constant of the $R_{act}C_{dl}$ branch.

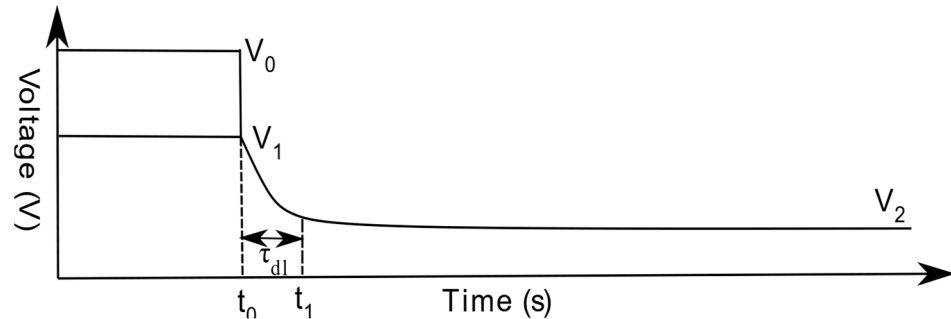


Figure 8. Nature voltage response [50].

The second method (SI) derives the parameters of the Randles–Warburg circuit, shown in Figure 7, when the concentration losses are considered. First, this technique uses the NVR method to determine the ohmic resistance R_{ohm} , and other parameters: R_{act} , C_{dl} , and Warburg impedance (Z_{wbg}) which represent the losses of concentration, are derived by an identification system using pseudo-random binary sequence excitation (PRBS) [53,56].

3.2. Semi-Empirical Approach

The most semi-empirical approach in the literature is based on electrochemical, thermodynamic, and empirical laws. Most of the semi-empirical methods reported in the literature are static models, neglecting the dynamic behavior of PEM EL.

3.2.1. Static Modeling

The static model of a PEM EL can be represented mathematically using an equation (Equation (13)), which defines the cell voltage of the PEM EL as the sum of the reversible voltage and various overvoltage (ohmic overvoltage, activation overvoltage, and diffusion overvoltage at both the anode and cathode).

$$V_{cell} = E_{rev} + V_{ohm} + V_{act} + V_{diff} \quad (13)$$

Reversible Voltage

The reversible voltage is the minimum potential required between the electrodes to split the water molecules into oxygen and hydrogen, as defined by the Nernst equation.

$$E_{rev} = E_{rev}^0 + \frac{RT_{cell}}{2F} \ln \left(\frac{a_{H_2} a_{O_2}^{1/2}}{a_{H_2O}} \right) \quad (14)$$

Equation (14) can be given by two general forms when oxygen and hydrogen are considered pure gases, and water is assumed to exist only in liquid form (the water vapor present at the anode and the cathode is neglected). In this case, $a_{H_2O} = 1$ [57].

$$E_{rev} = E_{rev}^0 + \frac{RT_{cell}}{2F} \ln(p_{H_2} p_{O_2}^{1/2}) \quad (15)$$

If the partial pressure of hydrogen equals the partial pressure of oxygen, we can simplify Equation (15) as:

$$E_{rev} = E_{rev}^0 + \frac{3RT_{cell}}{4F} \ln(p) \quad (16)$$

The second form (Equation (17)) is used when the applied liquid water is assumed to be equal to the saturated vapor pressure [58–60].

$$E_{\text{rev}} = E_{\text{rev}}^0 + \frac{RT_{\text{cell}}}{2F} \ln \left(\frac{p_{\text{H}_2} p_{\text{O}_2}^{1/2}}{p_{\text{H}_2\text{O}}^{\text{sat}}} \right) \quad (17)$$

The first term (E_{rev}^0) represented the standard reversible potential; many authors took $E_{\text{rev}}^0 = 1299$ [4,56,61–65], but it is only true under standard conditions ($p = 1$ atm, $T = 298.15$ K). This potential decreases as the temperature increases. The empirical equations used to represent the dependence of the standard reversible voltage on temperature are summarized in five expressions. The first, Equation (18), was developed by LeRoy [66] for the alkaline electrolyzer, and after that, many works have used the same expression for PEM EL [67–73]; Dale [58] also followed the same LeRoy approach to derive another similar expression (Equation (19)) and was quoted by several authors. Recently, Lopes [74] approximated the temperature dependence of the standard reversible voltage by a third order polynomial (Equation (20)). Additionally, several authors adopted a simple linear empirical in Equation (21) [6,57,60,61,75–81].

$$E_{\text{rev}}^0 = 1.5184 - 1.5421 \times 10^{-3}T + 9.523 \times 10^{-5}T \ln T + 9.84 \times 10^{-8}T^2 \quad (18)$$

$$E_{\text{rev}}^0 = 1.5241 - 1.2261 \times 10^{-3}T + 1.1858 \times 10^{-5}T \ln T + 5.6692 \times 10^{-7}T^2 \quad (19)$$

$$E_{\text{rev}}^0 = 1.449 - 6.39 \times 10^{-4}T - 4.592 \times 10^{-7}T^2 + 1.46 \times 10^{-10}T^3 \quad (20)$$

$$E_{\text{rev}}^0 = 1.229 - 8.5 \times 10^{-4}(T - 298.15) \quad (21)$$

Finally, Reference [82] is based on Gibbs' free energy change (Equation (22)) to develop the standard reversible voltage.

$$E_{\text{rev}}^0 = \frac{\Delta G^0}{2F} = \frac{\Delta H^0 - \Delta S^0}{2F} \quad (22)$$

If considering that the temperature at the cathode and the anode are equal ($T_{\text{an}} = T_{\text{cat}} = T$), we can deduce the standard Gibbs' free energy changes as:

$$\Delta G^0 = (H_{\text{H}_2}(T) + 0.5H_{\text{O}_2}(T) - H_{\text{H}_2\text{O}}(T)) - T(S_{\text{H}_2}(T, p) + 0.5S_{\text{O}_2}(T, p) - S_{\text{H}_2\text{O}}(T, p)) \quad (23)$$

Enthalpy and entropy of hydrogen, oxygen, and water have been evaluated using the empirical correlation with temperature and pressure defined in (Equations (24) and (25)), with a_i , b_i , c_i , and d_i as the fitting coefficients [82,83].

$$H(T) = a_i T + \frac{4}{5}b_i T^{5/4} + \frac{2}{3}c_i T^{3/2} + \frac{4}{7}d_i T^{7/4} \quad (24)$$

$$S(T, p) = a_i \ln T + 4b_i T^{1/4} + 2c_i T^{1/2} + \frac{4}{3}d_i T^{3/4} - R \ln p \quad (25)$$

The partial pressures p_{H_2} , p_{O_2} , and $p_{\text{H}_2\text{O}}^{\text{sat}}$ are necessary to calculate the reversible voltage. Most of the authors have based their work on Dalton's law (Equations (26) and (27)) and the three following assumptions to derive these partial pressures:

A1: Hydrogen and gaseous oxygen behave like ideal gases;

A2: At the anode, there is only water and oxygen vapor, and also at the cathode, there is only water and hydrogen vapor;

A3: The solubility of hydrogen and oxygen in water is assumed negligible.

$$p_{\text{H}_2} = p_{\text{cat}} - p_{\text{H}_2\text{O}}^{\text{sat}} \quad (26)$$

$$p_{\text{O}_2} = p_{\text{an}} - p_{\text{H}_2\text{O}}^{\text{sat}} \quad (27)$$

The total pressure at the cathode p_{ca} and the anode p_{an} was measured from the gas separator. Many equations can calculate the saturated vapor pressure $p_{\text{satH}_2\text{O}}$. The August–Roche–Magnus formula (Equation (28)) and Antoine equation (Equation (29)) remain the most popular [43,57,59,67,78].

$$p_{\text{H}_2\text{O}}^{\text{sat}} = 6.1078 \times 10^{-3} \exp \left[17.694 \times \frac{T - 273.15}{T - 34.85} \right] \quad (28)$$

$$p_{\text{H}_2\text{O}}^{\text{sat}} = 10^{B - \frac{C}{D+T}} \quad (29)$$

Another analytical method developed in [82] has been used to calculate the partial pressure based on the substance flow inside the PEM EL cells.

Ohmic Losses

The ohmic losses in the cells are due to two components and their ionic resistance of the membrane (R_{ohm}), and electronic resistance of the electrodes and bipolar plates (R_{ele}). In the literature, the ohmic resistance is calculated using empirical and analytical methods. For the empirical method, the ohmic resistance is approximated by applying electrochemical techniques (see dynamic model section), but this method gives authentic ohmic resistance only under steady operating conditions. Some authors have estimated the ionic resistance of the membrane (neglecting electronic resistance) by empirical correlation with temperature. Table 1 summarizes these empiric expressions and their references.

For the analytical method, the ohmic resistance is calculated as:

$$R_{\text{ohm}} = R_{\text{mem}} + R_{\text{ele}} : \begin{cases} R_{\text{mem}} = \frac{\delta_{\text{mem}}}{A_{\text{mem}} \sigma_{\text{mem}}} \\ R_{\text{ele}} = \rho_{\text{el}} \frac{\ell_{\text{ele}}}{A_{\text{ele}}} \end{cases} \quad (30)$$

The authors in study [82] have modeled electronic resistance (electrodes and bipolar plates) as a network resistance and calculated them by analogies of electrical circuits. This approach is complex because it requires knowledge of each component's resistivity and geometric dimensions. However, the contribution of the electronic resistance to the ohmic losses remains very low compared to the ionic resistance [81]. In this case, the conductivity of the membrane is the key to calculating the ionic resistance. A popular empirical expression defines the conductivity depending on cell temperature and membrane water content (Equation (31)).

$$\sigma_{\text{mem}} = 5.14 \times 10^{-3} \lambda_{\text{mem}} - 3.26 \times 10^{-3} \exp \left[1268 \left(\frac{1}{303} - \frac{1}{T} \right) \right] \quad (31)$$

Table 1. Ohmic empirical methods.

Empirical Method	Ohmic Resistance (Unit)	Reference
EIS technique	Constant value (Ohm)	[46,49,50,72,84,85]
CI technique	Constant value (Ohm)	[51,53,56]
Empirical correlation	$R_{\text{ohm}} = 9.12 \times 10^{-3} \exp \left(\frac{1109}{T} \right)$ (Ohm.cm ²)	[81]

Unlike a PEM fuel cell, water is present in large quantities at the anode and the cathode in PEM EL. For this reason, many researchers considered the membrane fully hydrated and assumed that the membrane water content is constant (up to 14) [4,7,63,75,76,81,82,86–90], or used a conductivity simplified expression which depends only on the cell temperature (Equation (32)). For more precision, some works give an empirical expression of membrane water content as summarized in Table 2.

$$\sigma_{\text{mem}} = \sigma_{\text{ref}} \exp \left[E_{\text{pro}} \left(\frac{1}{T_{\text{ref}}} - \frac{1}{T} \right) \right] \quad (32)$$

The membrane conductivity can be obtained by fitting algorithms or other expressions as summarized in Table 3.

Table 2. Membrane water content equations.

Expression	Reference
$\begin{cases} \lambda_{\text{mem}} = 0.043 + 17.8 a - 39.85 a^2 + 36 a^3 & 0 < a \leq 1 \\ \lambda_{\text{mem}} = 14 + 1.4(a - 1) & 1 < a \leq 3 \end{cases}$	[31,32,91–94]
$\lambda_{\text{mem}} = \frac{\lambda_{\text{an}} - \lambda_{\text{cat}}}{\delta_m} x + \lambda_{\text{cat}}$	[95,96]
$\lambda_{\text{mem}} = 0.5(\lambda_{\text{an}} + \lambda_{\text{cat}})$	[97]
$\lambda_{\text{mem}} = 0.08533T - 6.77632$	[25]
$\lambda_{\text{mem}} = 0.3 + 10.8 \times \left(\frac{P_{\text{H}_2\text{O}}}{P_{\text{H}_2\text{O}}^{\text{sat}}} \right) - 16 \times \left(\frac{P_{\text{H}_2\text{O}}}{P_{\text{H}_2\text{O}}^{\text{sat}}} \right)^2 + 14.1 \times \left(\frac{P_{\text{H}_2\text{O}}}{P_{\text{H}_2\text{O}}^{\text{sat}}} \right)^3$	[98]

Table 3. Membrane conductivity.

Expression	References
$\sigma_{\text{mem}} = 5.14 \times 10^{-3} \lambda_{\text{mem}} - 3.26 \times 10^{-3} \exp \left[1268 \left(\frac{1}{303} - \frac{1}{T} \right) \right]$	[4,7,25,31,32,59,63,69,75,76,80–82,86–97,99–102]
$\sigma_{\text{mem}} = \sigma_{\text{ref}} \exp \left[\frac{E_{\text{pro}}}{R} \left(\frac{1}{T_{\text{ref}}} - \frac{1}{T} \right) \right]$	[59,71,79]
$\sigma_{\text{mem}} = 4.80257 \times 10^{-2} + 8.15178 \times 10^{-4} (T - 273) + 5.1192 \times 10^{-7} (T - 273)^2$	[58]
$\sigma_{\text{mem}} = \frac{\varepsilon}{\zeta} \left[\frac{F^2}{RT} \left(D_{\text{H}^+}^{\Sigma} C_{\text{H}^+}^{\Sigma} + D_{\text{H}^+}^{\text{G}} C_{\text{H}^+} + \frac{D_{\text{H}^+}^{\text{w}} C_{\text{H}^+}}{1 + \delta_c} \right) \right]$	[43,82,89,94,100,103]
$\sigma_{\text{mem}} = 0.0013 \lambda_{\text{mem}}^3 + 0.0298 \lambda_{\text{mem}}^2 + 0.2658 \lambda_{\text{mem}} \exp \left[E_{\text{act}} \left(\frac{1}{353} - \frac{1}{T} \right) \right]$	[98]
$\sigma_{\text{mem}} = 2.29 \exp \left[-\frac{7829}{RT} \right]$	[89]
Constant value	[73,74,104,105]

Activation Losses

The activation overpotential arises from the electrochemical reaction's kinetics at the electrode's surface. This overpotential is related to the catalyst's materials, the active catalyst surface, and temperature. Generally, the activation overpotential is described by the Butler–Volmer equation (Equation (33)) or by the Tafel correlation (Equation (34)).

$$V_{\text{act}} = \frac{RT}{\alpha_{\text{an}} F} \sinh^{-1} \left(\frac{i}{2i_{0,\text{an}}} \right) + \frac{RT}{\alpha_{\text{cat}} F} \sinh^{-1} \left(\frac{i}{2i_{0,\text{cat}}} \right) \quad (33)$$

$$V_{\text{act}} = \frac{RT}{2\alpha_{\text{an}} F} \ln \left(\frac{i}{i_{0,\text{an}}} \right) + \frac{RT}{2\alpha_{\text{cat}} F} \ln \left(\frac{i}{i_{0,\text{cat}}} \right) \quad (34)$$

Indeed, the reaction kinetics of oxygen at the anode are very slow compared to the reaction kinetics of hydrogen at the cathode. Therefore, the contribution of overpotential activation at the cathode is neglected in many works [4,31,59,63,67,71,78,88,90,91,93,106–108].

The activation overpotential can be improved by correcting the electrode's roughness, which is translated to an active catalyst's larger site. There are other expressions in the literature used to represent the activation overpotential as shown in Table 4.

The charge transfer coefficient (CTC) and exchange current density (ECD) are essential electrochemical parameters to calculate the activation overpotential. For simplicity, most of the authors assumed that the CTC is constant or equal to the symmetric factor ($\alpha_{an} = \alpha_{cat} = 0.5$) (see Table 5). However, the operation temperature of PEM EL strongly affected the CTC. This effect is more important at the anode electrode. Moreover, an estimation error of CTC strongly influences the polarization curve and performance characteristics of PEM EL [57,58,109].

The exchange current density (ECD) has a radical effect on the activation overpotential. Many studies estimated ECD based only on the catalyst materials. We can observe from Table 5 that the choice of the ECD is not clear. For the same catalyst materials, we can find a big difference in ECD value estimates by different authors.

Additionally, the ECD strongly depends on the electrodes' roughness, concentration, the catalyst particles' dimension, and operating temperature [71,81,101]. Arrhenius expression (Equation (35)) is one of the most famous equations, which gives ECD as a function of temperature, activation energy, and exchange current density at reference conditions. A similar accurate expression represents the ECD as a function of precedent parameters and the roughness factor in Equation (36).

$$i_{0,an} = i_{0,an}^{ref} \exp \left[\frac{-E_{act,an}}{R} \left(\frac{1}{T} - \frac{1}{T_{ref}} \right) \right] \quad (35)$$

$$i_{0,an} = \gamma_{M,an} i_{0,an}^{ref} \exp \left[\frac{-E_{act,an}}{R} \left(\frac{1}{T} - \frac{1}{T_{ref}} \right) \right] \quad (36)$$

The different expressions of ECD and their references are listed in Table 6, as well as activation energy, exchange current density at reference conditions i_0^{ref} , and roughness factor γ in Table 7. Even though the correlation expression of ECD with the temperature is adopted, the activation energy and ECD at reference conditions must be determined.

Table 4. Activation overpotential.

Expressions	Activation Overpotential at Cathode	References
$V_{act} = \frac{RT}{2\alpha_{an}F} \ln \left(\frac{i}{i_{0,an}} \right)$	Neglected	[4,31,63,90,91,93,106,107,110]
$V_{act} = \frac{RT}{F} \left[\sinh^{-1} \left(\frac{i-i_v}{2i_{0,an}} \right) + \sinh^{-1} \left(\frac{i}{2i_{0,cat}} \right) \right]$	Considered	[79]
$V_{act} = \frac{RT}{\alpha_{an}F} \sinh^{-1} \left(\frac{i}{2i_{0,an}} \right) + \frac{RT}{\alpha_{cat}F} \sinh^{-1} \left(\frac{i}{2i_{0,cat}} \right)$	Considered	[32,43,75,76,78,80–82,86,87,97,98,101,111,112]
$V_{act} = \frac{RT}{2\alpha_{an}F} \sinh^{-1} \left(\frac{i}{2i_{0,an}} \right) + \frac{RT}{2\alpha_{cat}F} \sinh^{-1} \left(\frac{i}{2i_{0,cat}} \right)$	Considered	[6,57,58,62,73,74,80,96,105,113]
$V_{act} = \frac{RT}{2\alpha_{an}F} \ln \left(\frac{i}{i_{0,an}} \right) + \frac{RT}{2\alpha_{cat}F} \ln \left(\frac{i}{i_{0,cat}} \right)$	Considered	[89,94,109,110]
$V_{act} = \frac{RT}{2\alpha_{an}F} \ln \left(\frac{i}{i_{0,an} \gamma_{an}} \right)$	Neglected	[88]
$V_{act} = \frac{RT}{\alpha_{an}F} \sinh^{-1} \left(\frac{i}{2i_{0,an}} \right) + \frac{RT}{\alpha_{an}F} \beta_{an} i^3$	Neglected	[78]
$V_{act} = \frac{RT}{\alpha_{an}F} \sinh^{-1} \left(\frac{i}{2i_{0,an}} \right)$	Neglected	[108]
$V_{act} = \frac{RT}{2\alpha_{an}F} \sinh^{-1} \left(\frac{i}{2i_{0,an}} \right)$	Neglected	[59,67]
$V_{act} = \frac{RT}{\alpha_{an}F} \sin^{-1} \left(\frac{i}{2\gamma_{an}i_{0,an}} \right) + \frac{RT}{\alpha_{cat}F} \sin^{-1} \left(\frac{i}{2\gamma_{cat}i_{0,cat}} \right)$	Considered	[60]

Table 5. Fitted parameters of activation overpotential.

$i_{0,an}$ (A.cm ⁻²) (Anode Catalyst)	$i_{0,cat}$ (A.cm ⁻²) (Cathode Catalyst)	α_{an} (Per unit)	α_{cat} (Per unit)	Operation Temperature (Kelvin)	Operation Pressure (bar)	References
10^{-12} – 10^{-9} (Pt)	10^{-4} – 10^{-3} (Pt)	0.5	0.5	353	—	[104]
0.76×10^{-5} – 4.93×10^{-5} (Pt)	0.18–0.39 (Pt)	0.1–0.6	0.5	283–333	10	[58]
4.2×10^{-3} – 5×10^{-4} (Pt)	0.179–0.433 (Pt)	0.179–0.433	0.5	293–333	10	[57]
0.13×10^{-3} (—)	X	0.452	X	353	—	[4]
10^{-13} – 10^{-6} (Ir-Ru)	0.025–0.1568 (Pt)	0.5	0.5	313–328	1–70	[82]
3.348×10^{-6} (—)	4.957×10^{-2} (—)	0.42	0.5	353	1	[74]
Cal (Pt)	Cal (Pt)	0.5	0.5	300–353	1–5	[95]
0.1548×10^{-2} (—)	0.3539×10^{-1} (—)	0.7178	0.6395	300–303	1	[105]
Cal (—)	X	0.5	X	—	—	[59]
Cal (—)	X	0.5	X	—	—	[71]
1×10^{-10} (—)	1×10^{-3} (—)	2	0.5	328	100	[86]
1×10^{-6} (Pt)	0.29 (Pt)	0.1	0.9	293	1	[94]
10^{-9} – 10^{-12} (Pt)	10^{-3} – 10^{-4} (Pt–Ir)	0.5	0.5	313–353	—	[7]
1.573×10^{-8} – 6.667×10^{-10} (With $\gamma_{an} = 150$) (—)	X	0.648–0.655	X	313–353	—	[88]

Table 5. Cont.

$i_{0,an}$ (A.cm ⁻²) (Anode Catalyst)	$i_{0,cat}$ (A.cm ⁻²) (Cathode Catalyst)	α_{an} (Per unit)	α_{cat} (Per unit)	Operation Temperature (Kelvin)	Operation Pressure (bar)	References
1×10^{-7} (Pt)	1×10^{-1} (Pt)	0.8	0.25	283–363	10–90	[81]
1×10^{-6} (—)	1×10^{-1} (—)	2	0.5	353	13.6	[76]
1×10^{-9} – 8×10^{-7} (Pt)	3×10^{-3} (Pt)	0.5	0.5	303–353	—	[79]
1×10^{-7} (—)	2×10^{-3} (—)	2	0.5	280–360	1–350	[32]
1.65×10^{-8} (—)	0.09 (—)	0.5	0.5	297.6–310	13.6	[114]
2.27×10^{-7} – 1.53×10^{-6} (—)	4.9×10^{-2} – 1.05×10^{-1} (—)	0.5	0.5	298–323	—	[69]
0.111 (—)	0.653 (—)	0.186	0.5	343	20	[78]
Cal (Ir–O ₂)	Cal (Pt)	—	—	313–353	1–30	[101]
2.472–1.43 (—)	2754–6024	0.8433–0.9484	0.8911–0.5491	298–333	1	[99]
Cal (—)	X	0.5	X	318–353	70–155	[108]
1×10^{-10} (—)	1×10^{-3} (—)	0.5	0.5	293–353	1–200	[89]
Cal (Pt)	Cal (Pt)	0.5	0.5	443	1	[73]
Cal (Pt)	Cal (IrO ₂)	1.2	0.5	353	1	[43]
Cal (Pt–IrO ₂)	X	0.7353	X	303–333	15–35	[43]

Table 5. Cont.

$i_{0,an}$ (A.cm ⁻²) (Anode Catalyst)	$i_{0,cat}$ (A.cm ⁻²) (Cathode Catalyst)	α_{an} (Per unit)	α_{cat} (Per unit)	Operation Temperature (Kelvin)	Operation Pressure (bar)	References
4.5756×10^{-7} (—)	X	0.5316	X	353	13.44	[90]
Cal (Pt-IrO ₂)	X	0.7353	X	303–333	15–35	[67]
1×10^{-6} – 1×10^{-1} (—)	0.01–10 (—)	0.5	0.5	333–368	1–40	[6]
1×10^{-7} (Pt-Ir)	1×10^{-3} (Pt)	0.5	0.5	293–353	1–20	[109]
1×10^{-12} – 1×10^{-8} (Pt)	1×10^{-3} –10 (Pt)	0.5	0.5	313–353	1–70	[80]
Cal (—)	Cal (—)	0.5	0.5	353	—	[96]
1.381×10^{-5} (—)	4.64×10^{-3} (—)	2	0.5	293	1	[97]
1.65×10^{-18} (—)	0.09 (—)	—	—	288	7	[111]
Cal (Ir-O ₂)	Cal (Pt)	0.5	0.5	353	—	[61]

—: not mentioned, X: the cathodic overpotential is neglected at the cathode, Cal: exchange current density is calculated using the physical law.

Tables 6 and 7 show that these parameters vary from one author to another, which is normal as the catalyst material, roughness factor, reference conditions, and fitted conditions may differ. Therefore, identifying these parameters through appropriate methods remains the best approach to derive them.

Diffusion Overpotential/Mass Transport Overpotential/Concentration Overpotential

The PEM EL utilizes water (H_2O_{in}) as the primary reactant for the production of hydrogen and oxygen through the process of electrolysis. The transport of water into the cell is due to three distinct phenomena, as illustrated in Figure 9: concentration gradient (H_2O_{diff}), pressure gradient (H_2O_{pe}), and electro-osmotic drag (H_2O_{eod}). The products of hydrogen (H_{2out}) and oxygen (O_{2out}) are then removed from the membrane–electrode interface via the porous electrodes and transported to the channels. At the anode, a portion of the water exits the cell (H_2O_{out}), while another portion crosses the membrane and is removed from the cell at the cathode [81,82,86,99]. As the mass flow rate increases, a diffusion overpotential may occur as a result of limitations in mass transport through the porous electrodes. This phenomenon is particularly significant at high current densities, as oxygen bubbles can accumulate on the membrane surface, thereby impeding the transport of water to the active surface area [57,81,82,93,97].

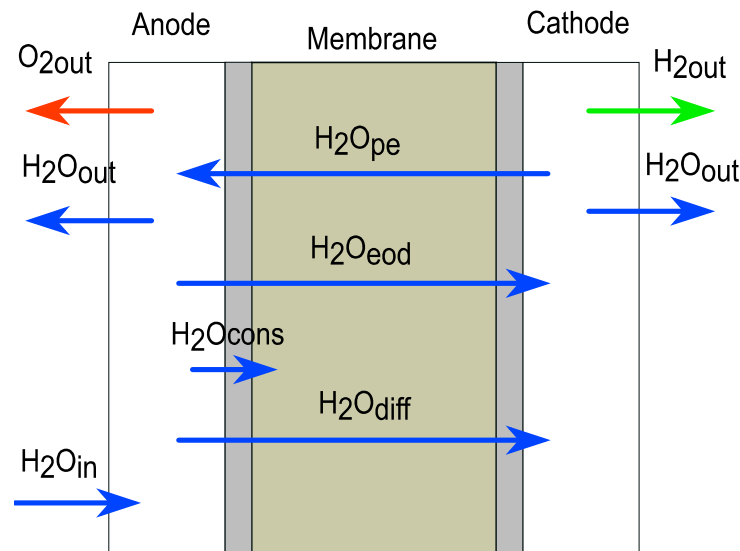


Figure 9. Water transport in PEM EL cell.

The diffusion overpotential can be modeled by applied Nernst equation in both electrodes:

$$V_{diff} = \frac{RT}{4F} \ln\left(\frac{C_{O_2,me}}{C_{O_2,me,0}}\right) + \frac{RT}{2F} \ln\left(\frac{C_{H_2,me}}{C_{H_2,me,0}}\right) \tag{37}$$

where Fick’s law describes the concentration of oxygen and hydrogen at the membrane–electrode interface; the theoretical analysis used to develop the diffusion overpotential is not included in this study. More details can be found in [76,81,82].

Table 6. Exchange current density expression.

At the Anode ($i_{0,an}$)	At the Cathode ($i_{0,cat}$)	References
$i_{0,an}(T) = e \times \ln\left(f \times \frac{1000}{T}\right)$ with ($e = 0.3037$ and $f = -0.0856$)	Not considered	[108]
$i_{0,an} = \gamma_{M,an} i_{0,an}^{ref} \exp\left[\frac{-E_{act,an}}{R} \left(\frac{1}{T} - \frac{1}{T_{ref}}\right)\right]$	$i_{0,cat} = \gamma_{M,cat} i_{0,cat}^{ref} \exp\left[\frac{-E_{act,cat}}{R} \left(\frac{1}{T} - \frac{1}{T_{ref}}\right)\right]$	[43,101]
$i_{0,an} = i_{0,an}^{ref} \exp\left[\frac{-E_{act,an}}{R} \left(\frac{1}{T} - \frac{1}{T_{ref}}\right)\right]$	$i_{0,an} = i_{0,cat}^{ref} \exp\left[\frac{-E_{act,an}}{R} \left(\frac{1}{T} - \frac{1}{T_{ref}}\right)\right]$	[59,61,71,73,95,96,110]

Table 7. Exchange current density at reference conditions, activation energy, and roughness factor.

Anodic Catalyst	$i_{0,an}^{ref}$ (A·cm ⁻²)	$E_{act,an}$ (Kj·mol ⁻¹)	$\gamma_{M,an}$ (per unit)	Cathodic Catalyst	$i_{0,cat}^{ref}$ (A·cm ⁻²)	$E_{act,cat}$ (Kj·mol ⁻¹)	$\gamma_{M,cat}$ (per unit)	References
Pt	1×10^{-11}	76	N.C	Pt	1×10^{-3}	18	N.C	[95,115]
—	2×10^{-12}	52.649	N.C	—	X	X	N.C	[110]
IrO ₂	5.35×10^{-7}	15	100	Pt	1×10^{-3}	18	40	[101]
Pt	8.4×10^{-11}	76	N.C	Pt	3224	18	N.C	[73]
(Pt – IrO ₂)	1.08×10^{-18}	52.994	N.C	X	X	X	X	[59,67]
—	1.7×10^1	76	N.C	—	4.6×10^{-1}	18	N.C	[96]
IrO ₂	—	62.836	N.C	Pt	—	24.359	N.C	[61]

—: not mentioned, N.C: not considered, X: the cathodic activation is neglected.

In reference [116], Fontes has suggested a simple expression of diffusion overpotential for the fuel cell in Equation (38). Then, several authors applied it for PEM EL [4,36,63,90,91,93]. This formula depends on the parameter called diffusion limit current density, which means the diffusion will stop at this value (hydrogen and oxygen production stopped at limited current density) [36,116].

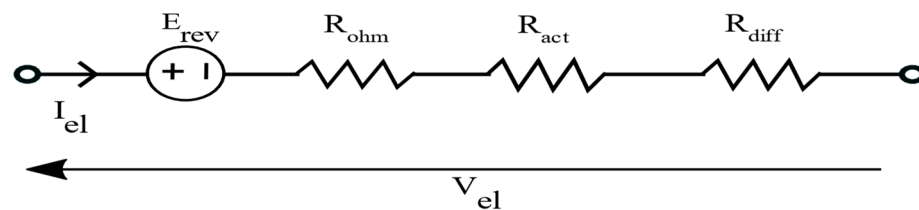
$$V_{diff} = \frac{RT}{2kF} \ln \left(1 + \frac{i}{i_{lim}} \right) \quad (38)$$

In the literature, some other formulas of diffusion overpotential are summarized in Table 8 with their references.

As mentioned above, the diffusion losses were important, especially at high current density, but fortunately, PEM ELs work under a nominal condition to achieve high efficiency. For that reason, many models have neglected the diffusion overpotential at operation current density [7,31,32,57–59,61,62,67,69,71,73–75,77–79,87,88,95–97,104–107,110,111,114,117].

Finally, the semi-empirical model can be transformed into EEC, consisting of a voltage source representing the reversible voltage E_{rev} , and three series of resistors, R_{ohm} , R_{act} , and R_{diff} which represent the ohmic, activation, and diffusion losses, respectively (Figure 10). The activation and diffusion overpotential have a nonlinear voltage-current density behavior. In this case, the differential resistance is useful to derive R_{act} and R_{diff} [79,104,117]:

$$\begin{cases} R_{act} = \frac{dV_{act}}{di} \\ R_{diff} = \frac{dV_{diff}}{di} \end{cases} \quad (39)$$

**Figure 10.** Equivalent electrical circuit based on the static semi-empirical modeling of PEM EL.

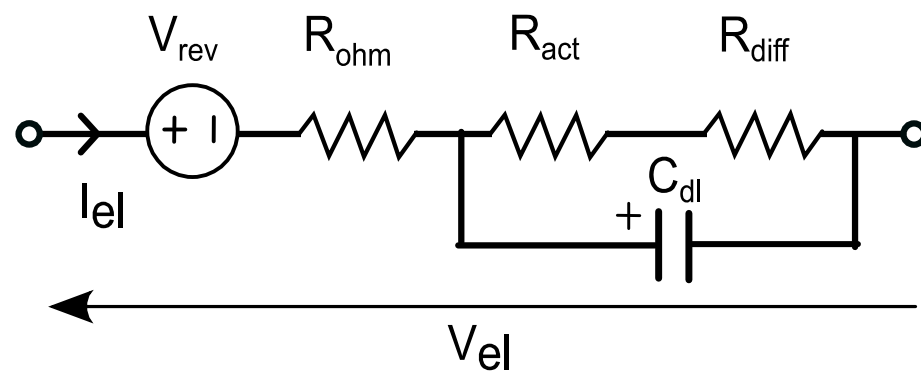
3.2.2. Dynamic Modeling

Most of the semi-empirical models reported in literature are static models, neglecting the dynamic behavior of PEM EL. However, these models are only valid if the PEM EL operates at a constant operating current (unchangeable operational current). Recently, in study [20], it was shown that during an abrupt variation of the input current, the error between the static model and the experimental data was greater than 15%, and that this was particularly significant during transient operation. In contrast, for the dynamic model, the error did not exceed 4%. However, in most cases, PEM EL is powered by intermittent energy sources such as photovoltaic panels or wind turbines, which can result in sudden variations in energy input, therefore, taking into account the dynamics of the system is more accurate and reliable for predicting the behavior of PEM EL in such cases.

Table 8. Diffusion overpotential.

Expression	References
$V_{\text{diff}} = \frac{RT}{4F} \ln\left(\frac{C_{\text{O}_2,\text{me}}}{C_{\text{O}_2,\text{me},0}}\right) + \frac{RT}{2F} \ln\left(\frac{C_{\text{H}_2,\text{me}}}{C_{\text{H}_2,\text{me},0}}\right)$	[6,43,60,76,80–82,86,94,99,101,109]
$V_{\text{diff}} = \frac{RT}{2\kappa F} \ln\left(1 + \frac{i}{i_{\text{Lim}}}\right)$	[4,63,90,91,93,118]
$V_{\text{diff_an,cat}} = i^2 \left[\mu_1 \left(\frac{i}{i_{\text{max}}} \right)^{\mu_2} \right]$	[95]
$V_{\text{diff}} = \frac{RT}{4F} \ln\left(1 - \frac{i}{i_{\text{Lim},\text{O}_2}}\right) + \frac{RT}{2F} \ln\left(1 - \frac{i}{i_{\text{Lim},\text{H}_2}}\right)$	[108]
$V_{\text{diff}} = \frac{RT}{2\alpha_{\text{an}}F} \ln\left(\frac{i_{\text{Lim}}}{i_{\text{Lim}} - i_{\text{an}}}\right)$	[89]

As mentioned in the previous section, the EIS and CI techniques introduced an equivalent capacitor in their models. This capacitor was explained by the accumulation of charges (electrons and protons) at the cell's electrode/electrolyte surface, called double-layer charging capacitance [92,119–124]. In the end, the dynamic model is represented by the same previous static semi-empirical model, adding a capacitor in parallel with the activation and diffusion resistors. In case the diffusion losses have been neglected, the capacitor remains only parallel with the activation resistor as shown in Figure 11 [14,15,19,20,25,63,74,92,125].

**Figure 11.** EEC of dynamic semi-empirical model.

4. PEM EL Sub-Models

The PEM EL efficiency is an important key to indicating and improving the performance of PEM EL and the overall system. Usually, the electrical models, energy efficiency, gas production, and water consumption of the PEM EL are affected by temperature and pressure. Developing the sub-models to provide these magnitudes are crucial to obtain accurate models and necessary for monitoring and controlling these quantities to avoid any damage and malfunction of PEM EL [25,32]. This subsection is devoted to highlighting and discussing the sub-models such as the thermal sub-model, the hydrogen storage tank sub-model, the mass flow of gas products, and efficiency of PEM EL which can be coupled with the PEM EL electrical model.

4.1. Thermal Sub-Model

Most scientific researchers have not been modeling the thermal behavior of the PEM EL stack. However, the polarization curve V-I, durability, gas flow rate, and efficiency are affected by temperature. So, the thermal management system is indispensable to obtain a precise model and optimize the efficiency of PEM EL, as well as the monitoring and regulation temperature required to avoid any damage caused by overheating.

In studies [72,106], PEM EL temperature is measured directly by thermocouple sensors on the cell body. Recently, Lee [126] measured the local temperature using the new technology of the micro temperature sensors (the thick polyimide film material whose resistance changes with temperature) embedded in PEM EL. However, the direct measurement of PEM EL stack temperature from an integrated sensor has a high maintenance cost and

can interrupt the electrolysis process if the sensors fail. For more reliability, a thermal sub-model can be added to the sensor measurement for redundancy, or we rely solely on the thermal model and external sensors to evaluate the PEM EL stack temperature.

According to reference [15], we estimate the stack temperature as a function of the ambient temperature and power supply to the PEM EL using the following algebraic equation:

$$T_{el} = T_{amb} + R_{th}(V_{el}I_{el}) \quad (40)$$

The thermal resistance R_{th} has been identified by applying the least squares regression on the measured temperature data. This method gives a good agreement with measurement data for the stack current range between 0.04 A/cm² and 0.16 A/cm², but the stack current range is between 0 A/cm² and 1 A/cm². Furthermore, this method does not describe the dynamic of stack temperature, which is necessary when temperature management systems are added to regulate the stack temperature.

Under a key assumption, the thermal gradient within PEM EL is negligible, leading many authors to adopt the lumped thermal capacitance to describe the dynamic behavior of PEM EL stack temperature.

From Figure 12 and the thermal energy balance, the dynamic of stack temperature can be formulated by an ordinary differential equation:

$$C_{th} \frac{dT_{stack}}{dt} = W_{e_heat} + \dot{N}_{H_2O}^{in} \Delta H_{H_2O} - \dot{Q}_{loss_amb} - \dot{Q}_{cool} - \sum_{j=H_2, O_2, H_2O} \dot{N}_j^{out} \Delta H_j^{out} \quad (41)$$

where the W_{e_heat} represents the electrical power dissipation as heat, $\dot{N}_{H_2O}^{in}$ is the heat of the water fed to the PEM EL, \dot{Q}_{loss_amb} represents the heat loss to the ambient, \dot{Q}_{cool} represents the heat removed from the electrolyzer stack by a cooling system, and the last term of Equation (41) represents the heat that leaves the stack with hydrogen, oxygen, and water.

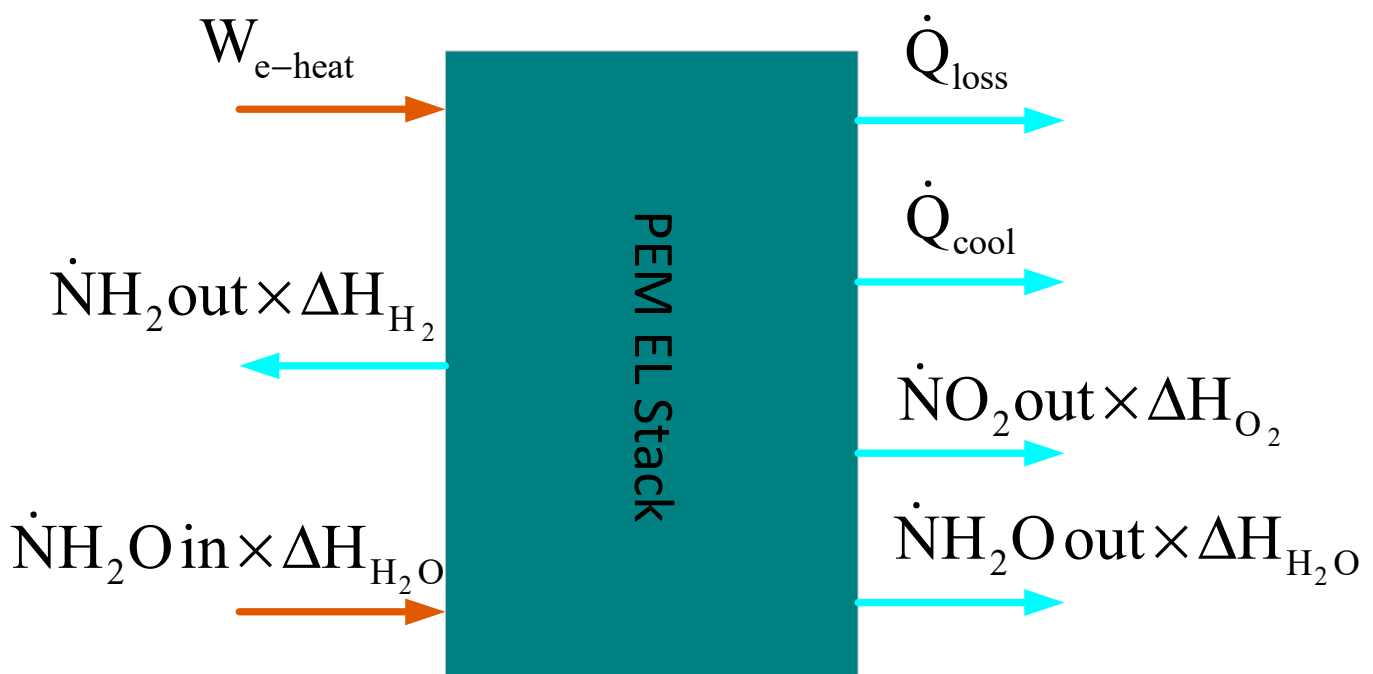


Figure 12. Heat transfer in a PEM EL [24].

Table 9 gathers all the previous literature regarding the thermal sub-model of PEM EL based on lumped thermal capacitance.

Table 9. Thermal model of PEM EL stack based on lumped thermal capacitance.

Expression	Cooling System	Parameters	References
$C_{th} \frac{dT_{stack}}{dt} = W_{e_heat} - \dot{Q}_{loss}$ $\left\{ \begin{array}{l} W_{e_heat} = N_{cell}(V_{cell} - V_{th})I_{el} \\ \dot{Q}_{loss} = H(T_{stack} - T_{amb}) \\ \dot{N}_{H_2O}^{in} \Delta H_{H_2O} \text{ and } \sum_{j=H_2,O_2,H_2O} \dot{N}_j^{out} \Delta H_j^{out} \end{array} \right. \text{ Are neglected}$	Not included	C_{th} and h are identified using the nonlinear least squares method	[4,62,99]
$C_{th} \frac{d(T_{stack})}{dt} = \dot{Q}_{gen} - \dot{Q}_{loss} - \dot{Q}_{cool}$ $\left\{ \begin{array}{l} \dot{Q}_{gen} = N_{cell}(V_{cell} - V_{th})I_{el} \\ \dot{Q}_{loss} = \frac{T - T_{amb}}{R_{th}} \\ \dot{Q}_{cool} : \text{Not mentioned} \end{array} \right.$	Included	C_{th} and R_{th} estimated experimentally	[110]
$C_{th} \frac{dT_{stack}}{dt} = W_{e_heat} - \dot{Q}_{loss} - \dot{Q}_{cool}$ $\left\{ \begin{array}{l} W_{e_heat} = N_{cell}(V_{cell} - V_{th})I_{el} \\ \dot{Q}_{loss} = \frac{T - T_{amb}}{R_{th}} \\ \dot{Q}_{cool} = C_{th}^m (T_m^{out} - T_m^{in}) \end{array} \right.$	Included	Not mentioned	[107,111,127]
$C_{th} \frac{dT_{stack}}{dt} = W_{e_heat} + \dot{N}_{H_2O}^{in} \Delta H_{H_2O} - \dot{Q}_{cool} - \dot{Q}_{loss} - \sum_{j=H_2,O_2} \dot{N}_j^{out} \Delta H_j^{out}$ $W_{e_heat} = N_{cell}(V_{cell} - V_{th})I_{el}$ $\dot{N}_{H_2O}^{in} \Delta H_{H_2O} = (W_{pump,ele} \eta_{moto} R_{ele}) - (Q \Delta P_{pump})$ $\dot{Q}_{loss} = \frac{1}{R_{th}} (T - T_{amb})$ $\sum \dot{N}_j \Delta H = \dot{N}_{H_2} C_{pH_2} (T - T_{amb}) + \dot{N}_{O_2} C_{pO_2} (T - T_{amb})$ $\dot{Q}_{cool} = \text{Not mentioned}$	Included	C_{th} and R_{th} are identified using particle swarm optimization (PSO)	[59,67]

4.2. PEM EL Efficiency

The PEM EL efficiency can be defined as a ratio between useful and absorbed power (Equation (8)). This magnitude is related to the operating conditions [70,72,108,117]. Particularly when the PEM EL is coupled to intermittent energy sources (wide range of operating conditions), it is important to optimize the efficiency to improve PEM EL performance. Few works evaluated this key magnitude despite its importance. Recently, Hernández in [25], investigated the efficiency and specific energy consumption of the PEM EL. However, there are three types of efficiency: faraday, voltage, and PEM EL efficiency.

4.2.1. Faraday Efficiency

Faraday efficiency is a ratio between real and theoretical hydrogen flow because, in reality, the portion of hydrogen can be across the membrane from the cathode to the anode. This phenomenon is important at low current density. At operation conditions, many authors assumed it less than or equal to 1% [5,7,59,67,72,89,99,106,128]. However, some researchers have determined this magnitude using empirical or semi-empirical expressions. In studies [31,129,130], the internal current density and hydrogen loss (i_{lim}) were introduced as critical parameters and the magnitude was determined using Equation (42). In study [131], it was expressed in Equation (43) as a function of the flux density across the membrane of the hydrogen ($\Phi_{H_2}^{per}$) and oxygen ($\Phi_{O_2}^{per}$), and their theoretical molar flow rate (\dot{N}_{H_2} and \dot{N}_{O_2}), as well as an empirical expression (Equation (44)), was used to estimate the faraday efficiency as a function of an electrolyzer current [117,132–134], and finally, in study [108], which was based on the mass flow calculation to deduce the faraday efficiency as the difference between theoretical molar flow rate and molar flow back diffusion over theoretical molar flow (Equation (45)).

$$\eta_F = \frac{i - i_{loss}}{i} \quad (42)$$

$$\eta_F = 1 - \frac{\Phi_{H_2}^{per}}{\dot{N}_{H_2}} - 2 \frac{\Phi_{O_2}^{per}}{\dot{N}_{H_2}} \quad (43)$$

$$\eta_F = 96.5 \left[\exp \left(\frac{0.09}{I_{el}} - \frac{75.5}{I_{el}^2} \right) \right] \quad (44)$$

$$\eta_F = \frac{\dot{m}_{H_2,theo} - \dot{m}_{H_2,back}}{\dot{m}_{H_2,theo}} \quad (45)$$

In the preceding section, we discussed the energy efficiency of PEM EL. However, in order to obtain a more comprehensive assessment of the overall efficiency of PEM EL, it is crucial to consider the exergy efficiency. The exergy efficiency accounts for the availability of energy and the different losses, taking into consideration various magnitude such as heat loss, the temperatures of internal and external water, and reactant gases, water and gas pressures, mass flow rate, and current-voltage during operation [135,136]. It is noteworthy that this study does not investigate the exergy efficiency of the PEM EL cells.

4.2.2. Voltage efficiency

As mentioned previously, the reversible voltage at operation conditions (p , T) is the minimum voltage required to split water into hydrogen and oxygen, but this electrochemical process needs to absorb heat (endothermic process). The electrolyzer voltage must be greater than the reversible voltage called thermoneutral voltage V_{th} to obtain an isothermal process [25,28,32,66,137].

The voltage efficiency term describes the voltage lost due to irreversibility losses (energy lost as heat) and can be defined as a ratio between thermoneutral voltage and the real voltage applied to the PEM EL (Equation (46)). The voltage efficiency is always very

small compared to the faradic efficiency; consequently, the electrolyzer efficiency is still strongly affected by faradic efficiency [32,64,70].

$$\eta_v = \frac{V_{th}}{V_{cell}} \quad (46)$$

The PEM EL efficiency can be defined as a product of faraday efficiency and voltage efficiency (Equation (47)) [18,25].

$$\eta_{Cell} = \eta_F \eta_v \quad (47)$$

Additionally, several scientific researchers have defined PEM EL efficiency as high heating value voltage of hydrogen over real PEM EL voltage (Equation (48)) [19,32,74,138].

$$\eta_{Cell} = \frac{V_{HHV}}{V_{cell}} = \frac{1.482}{V_{cell}} \quad (48)$$

4.3. Mass Flow of Gas Products and Water Consumed

According to the faraday law, we can easily deduce the mass flow rate of hydrogen and oxygen products as shown in the following expressions:

$$\dot{N}_{O_2} = N_{cell} \frac{I_{el}}{4F} \eta_F \quad (49)$$

$$\dot{N}_{H_2} = \dot{N}_{H_2O} = N_{cell} \frac{I_{el}}{2F} \eta_F \quad (50)$$

4.4. Hydrogen Storage Tank Sub-Model

The hydrogen gas produced by PEM EL can be stored directly in the tanks so that they can be restored by the fuel cells when we need it or compressed at high pressure into liquid hydrogen to transport it. Assuming the hydrogen gas is ideal under a low-pressure storage process (hydrogen pressure less than 138 bar), the following equation can give the dynamic storage [32,36,106,132,134]:

$$P_{tank} = z \frac{N_{H_2} RT_{tank}}{M_{H_2} V_{tank}} + P_{tank_initial} \quad (51)$$

At high-pressure storage, the ideal gas assumption becomes inefficient in calculating the tank pressure. The Van der Waals equation (Equation (52)) is one of the favorite expressions used to estimate the hydrogen tank's pressure [77]:

$$P_{tank} = \frac{N_{H_2} RT_{tank}}{v_{tank} - b N_{H_2}} - a \frac{N_{H_2}^2}{v_{tank}^2} \quad (52)$$

where a and b are Van der Waals coefficients of hydrogen. Another expression called the Beattie–Bridgeman equation (Equation (53)) was also used to calculate the tank's pressure for real gases [107,139]:

$$P_{tank} = \frac{N_{H_2}^2 RT_{tank}}{v_{tank}^2} \left(1 - \frac{a_1 N_{H_2}}{v_{tank} T_{tank}^3} \right) \left[\frac{v_{tank}}{N_{H_2}} + a_2 \left(1 - \frac{a_3 N_{H_2}}{v_{tank}} \right) \right] - \frac{a_4 \left(1 - \frac{a_5 N_{H_2}}{v_{tank}} \right) N_{H_2}^2}{v_{tank}^2} \quad (53)$$

where a_1 – a_7 are empirical parameters.

5. DC/DC Power Converter for PEM EL

In a hydrogen production system, the PEM EL cannot be powered directly, and it frequently requires power electronic converters for interfacing the PEM EL and renewable energy sources (RES) or the power grid. There are many power converter topologies (i.e., AC/DC converters, DC/DC converters, and AC/DC followed by DC/DC converters) that

can be used to supply PEM EL, generally depending on the types of energy sources (i.e., RES, AC grid power or DC bus) and voltage level which are required for the PEM EL.

In the case of PEM EL powered by wind turbines, AC grid, or AC bus configuration, it is indispensable to use AC/DC converters (i.e., uncontrolled rectifiers, controlled rectifiers). We can use AC/DC converters directly to supply PEM EL in the first case. However, the output voltage of these topologies is usually very high compared to the PEM EL voltage [27]. We can add a step-down transformer between the AC voltage sources and AC/DC converter to remedy this problem. However, this solution increases the global cost and decreases the total efficiency of the hydrogen production system. Again, this topology has some drawbacks, and it has a high current ripple which increases the specific power consumption of PEM EL, and poor power quality and power factor due to the presence of harmonics which requires adding the passive harmonic filters or active harmonic filters, which will complicate the converter design. Finally, in an energy management system or an autonomous renewable energy system based on the production of hydrogen from hybrid RES, the power grid, and RES supply of the DC bus via a suitable power converter, as well as PEM EL supplies by DC bus via DC/DC converter, this configuration has been the subject of considerable research [17,19,27,140–143]; also in this study, we will focus on the DC/DC converter interfacing PEM EL and DC bus. These drawbacks can be improved by using DC/DC converter after AC/DC converter [18]. Recently, some reviews have investigated differences in power converter topologies used for PEM EL [18,28]. In the second configuration, we will find the PEM EL powered by photovoltaic panels (PVs) via DC/DC converters (generally buck converters) with MPPT to extract the maximum of energy available to PVs.

Recently, in reference [27], the state-of-art is carried out on DC/DC converters adapted with PEM EL. First, this study shows that the step-down converters are used in most cases when the PEM EL is connected to the DC bus. In the second part, this study compared and evaluated the different step-down converters for PEM EL application (isolated and non-isolated step-down converters) in terms of meeting specific requirements: high energy efficiency, high current density, low conversion ratio, low current ripple, low electromagnetic interference, low cost, and continuity of service in the case of power switch failures [17,27,28]. The main result of this study shows that the Isolated Half-Bridge Converter (IHBC) and Interlaced Buck Converter (IBC) meet the main requirements mentioned above.

The IBC converter interests several researchers due to having a low current ripple and its ability to operate in the case of power switch failures. Unfortunately, this topology has two major drawbacks: high voltage conversion ratio, which makes the IBC not suitable for high voltage DC bus, and high voltage stress at the terminals of power switches [17,19,27,144]. In studies [16,17], an investigation on several IBC topologies shows that the three following modified conventional IBCs can be improved significantly regarding the voltage conversion ratio and energy efficiency without affecting the dynamic of the IBC: IBC with coupled winding (Figure 13), IBC with windings-cross-coupled inductors and passive-less clamp scheme (Figure 14), and interleaved-coupled buck converter with active-clamped circuits (Figure 15).

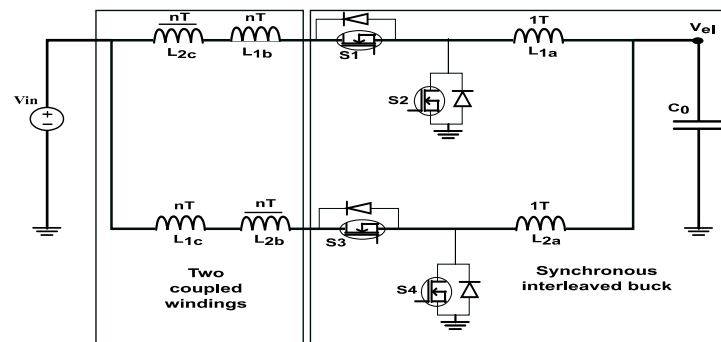


Figure 13. IBC with coupled winding [145].

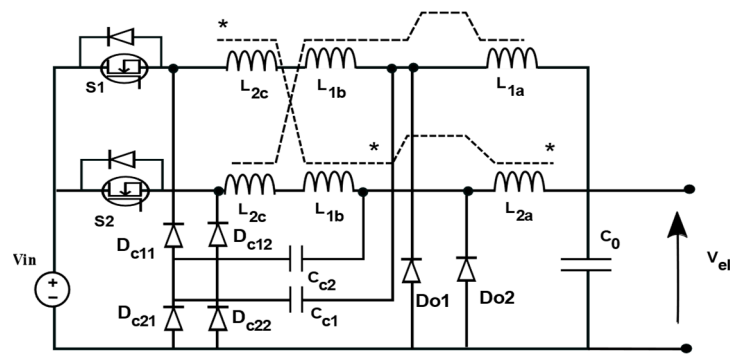


Figure 14. IBC with windings-cross-coupled inductors and passive-less clamp scheme [145].

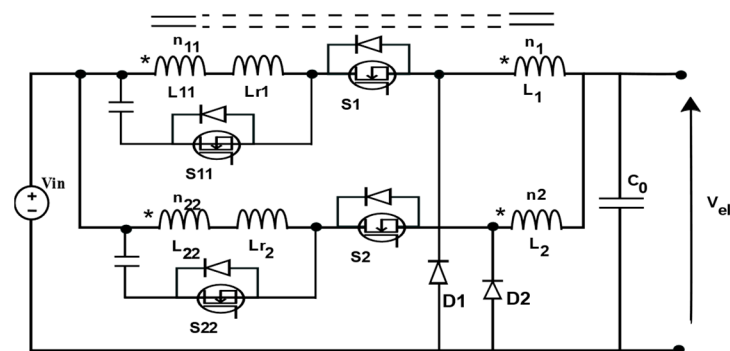


Figure 15. Interleaved-coupled buck converter with active-clamped circuits [145].

Increasing the switching frequency improves the current ripple, power density (i.e., decreases the filter volume and size), and dynamic performances of IBC. However, in return, it increases the switching losses at turn OFF and turn ON transition, losses due to the reverse recovery time of diodes, and the electromagnetic interferences [145–147]. These drawbacks can be improved using the above soft switching circuits. Moreover, several studies have proposed modifying the IBC by incorporating soft switching circuits to enhance its performance [145–152].

Through the previous investigation, we can consider the improved converter IBC as a good converter suitable for PEM EL because of its advantages. Notably, it has a low current ripple, the ability to keep working in case of switching failure, and low switching losses.

6. Control Strategy of DC-DC Converter–PEM EL Systems

The design of the controller for the DC/DC converter-PEM EL system is a crucial and essential step. The primary goal of the controller is to ensure the closed-loop stability of the entire system, while other objectives depend on the type of hydrogen production configuration (e.g., PVs-PEM EL, wind turbine-PEM EL, DC bus-PEM EL), and the controlled magnitude (e.g., hydrogen flow rate control, optimization of the energy efficiency of PEM EL, etc.).

In the literature, many kinds of control strategies have been adopted for different topologies and PEM EL models, as summarized in Table 10.

For DC bus configuration-PEM EL, the controller has been designed according to the following objective:

- Regulation of the hydrogen flow rate to its constant reference through the PEM EL current under a wide variation of operating conditions. The reference current can be determined as follows:

The hydrogen flow rate (m^3/h) can be deduced from Equation (54) and ideal gas law:

$$Q_{\text{H}_2-\text{v}} = \left(\eta_{\text{F}} \times \frac{N_{\text{cell}}RT}{2Fp_{\text{H}_2}} \times 3600 \right) I_{\text{el}} \quad (54)$$

Table 10. Different control strategies for different converter-PEM EL configurations.

Hydrogen Production Configuration	Modeling Methods of PEM EL	DC/DC Converter Used to Supply PEM EL	Magnitude Controlled	Control Law Strategy	References
PV-PEM EL	EIS (dynamic model)	Buck converter	Current regulator	Linear control (NM)	[49]
PEM EL-PEM FC	Model-based on experimental data (linear time invariance state space in discrete-time)	Buck converter	Voltage regulator	MPC with a disturbance's observer	[153]
PEM EL-Three-phase grid	Static linear model ($R_{\text{stack}}-V_{\text{stack}}$)	Phase-shifted full-bridge	Current regulator	PI control	[154]
PEM EL-DC bus	Dynamic linear model	IBC converter	Voltage regulator	SMC control with linear observer	[155]
PEM EL-DC bus	Dynamic linear model	IBC converter	Voltage regulator	SMC control	[156]
PEM EL-DC bus	Dynamic linear model	Quadratic buck converter	Current regulator	SMC control	[20]
PEM EL-DC bus	Static nonlinear model	Synchronous buck converter	Voltage regulator	PI control	[143]
PEM EL Three-phase grid	Static linear model	Phase-shift full-bridge converter	Current regulator	PI control	[157]
Micro wind generator-PEM EL	Static linear model	Full bridge converter	Current regulator	PI control	[158]
DC-bus PEM EL	Linear static model	Three-levelinterleaved DC-DC buck converter	Voltage control	PI control	[19]
High DC voltage RES sources	Dynamic linear model	Stacked interleaved buck converter	Voltage control	PI control	[119]
PV-PEM EL	Linear static model	Classical buck converter	Voltage control	PID control	[36]
PV-PEM EL	Nonlinear static model	Classical buck converter	Voltage control	PI control	[159]
DC-bus PEM EL	Linear static model	Stacked interleaved DC-DC buck converter	Combined with voltage control and current control	PID control	[21]
DC-bus PEM EL	Linear static model	Buck converter	Current control	ST- SMC control	[160]

The standardized hydrogen flow rate is usually expressed in standard liter per minute (slpm). We get the hydrogen flow rate in slpm by replacing the temperature and pressure with their values at standard conditions ($T = 298.15$ and $p = 1$ bar).

$$Q_{\text{H}_2-\text{slpm}} = (0.007608 \times \eta_{\text{F}} \times N_{\text{cell}}) I_{\text{el}} \quad (55)$$

Then, the reference current I_{el-ref} is found as a function of the desired hydrogen flow rate $Q_{H_2-slpm-ref}$:

$$I_{el-Ref} = \frac{Q_{H_2-slpm-Ref}}{0.007608 \times \eta_F \times N_{cell}} \quad (56)$$

- Control hydrogen flow rate through PEM EL current as shown above according to the state of charge of the hydrogen tank and hydrogen consumption by fuel cells.
- Regulate the PEM EL voltage to its reference voltage despite the DC bus voltage variation and the operation point variation.
- Some objectives can be added, such as ensuring equal current sharing between the three parallel legs when the IBC is used, etc.

To design the controller, most authors based their work on the average state-space model of DC/DC converter-PEM EL [55,143,155,156,158].

After identifying the control objectives and developing the mathematical model of the system, the last step is to design the controller. In study [143], PI linear control has been used to regulate the PEM EL voltage to its nominal voltage. Study [119] also used PI control to regulate the PEM EL voltage to its constant reference despite the input voltage variation. Likewise, in study [19], based on the PI control, the energy efficiency of the DC/DC converter-PEM EL system is optimized by regulating the PEM EL voltage to its optimal value. In study [20], Sliding Mode Control (SMC) was adopted as a nonlinear control method to handle the hydrogen flow rate through the PEM EL current according to the state of charge of the hydrogen tank and hydrogen consumption from fuel cells despite the operation condition variation. Additionally, studies [155,156] and SMC were chosen to regulate the PEM EL voltage to its constant reference value at the nominal operating point.

The PEM EL models we studied previously contain many unknown parameters that must be determined to design the controller or diagnose its health. The parameters were identified using the CI or EIS method for PEM EL models based on the Randles equivalent circuit and the Randles–Warburg equivalent circuit [49,53,56]. Additionally, for nonlinear static models, some authors have used nonlinear least squares regression to derive these parameters. Moreover, some other authors have based their work on particle swarm optimization (PSO) [4,59]. In studies [15,20,125], the linear dynamic model was proposed and identified the unknown parameters using linear least squares regression (LSR). These identification techniques and their references are summarized in Table 11.

In the literature, most of the methods dedicated to identifying the parameters of the PEM EL models are offline. In fact, the PEM EL parameters are strongly changing with energy input and operation conditions, and a slight parameter variation leads to a wide variation in the PEM EL voltage [6]. For more reliability, these parameters should be identified online. Several works use online parameter identification algorithms for fuel cells, such as [161], which has used adaptive recursive least square (ARLS) as a linear identification method to identify the parameters of the semi-empirical model. Study [134] has proposed three identification algorithms for three semi-empirical models, recursive least square (RLS) and Kalman Filter (KF) for linear identification and Extended Kalman Filter (EKF) for nonlinear identification. However, three recent studies have addressed this subject for the PEM EL. The first one [162] has been based on the model reference adaptive approach, which can be an online estimate of the time constant of the cathode reaction of PEM EL. Moreover, the last two studies [14,163] described the behavior of the parameters of the dynamic model as a function of the PEM EL current by a series of experiences. Then, from the observations the reversible voltage and membrane resistance as the constant value has been estimated. The other parameters (time constants and capacitances of the PEM EL model) behave like a Gaussian function, estimating these parameters as a current function using the normal law and linear relation between parameters.

Table 11. The identification techniques.

Model Adopted	Identification Method	Parameter's Vector	Mean Relative Error	References
Nonlinear static model	Nonlinear least square identification (NLS)	$\Phi = [R_{\text{mem}} \quad \alpha_{\text{an}} \quad i_0 \quad i_{\text{lim}} \quad \kappa]$	0.32%	[4]
Model-based on CI method	Current interruption (CI)	$\Phi = [R_{\text{mem}} \quad R_{\text{act}} \quad Z_{\text{wbg}} \quad C_{\text{dl}}]$	7.38%	[53,56]
Nonlinear static model	MATLAB identification tools	$\Phi = [\sigma_{\text{mem}} \quad \alpha_{\text{an}} \quad \alpha_{\text{cat}} \quad i_{\text{an}} \quad i_{\text{cat}}]$	0.11%	[62,99]
Nonlinear static model	Particle swarm optimization algorithm (PSO)	$\Phi = [R_{\text{mem}} \quad \alpha_{\text{an}} \quad i_{0,\text{an}}]$	2%	[59]
Linear dynamic model	Linear dynamic last square regression	$\Phi_{\text{LSR_static_model}} = [R_{\text{int}} \quad V_{\text{int}}]$ $\Phi_{\text{LSR_dynamic_model}} = [R_1 \quad R_2 \quad C_1 \quad C_2]$	15% for static model;4% for dynamic model	[15,20,125]
Linear dynamic model	EIS method	$\Phi = [R_{\text{mem}} \quad R_{\text{act}} \quad Z_{\text{wbg}} \quad C_{\text{dl}}]$	Not mentioned	[49]

The online identification of the parameters of the PEM EL model is crucial to develop a robust controller and the performance evaluations of PEM EL. As shown above, many methods have been used to control PEM EL with online parameter estimation of the static and dynamic PEM EL models. Moreover, the adaptive controls or the extended observer like Extended Kalman Filter (EKF) are needed to investigate them for the DC/DC converter-PEM EL system.

7. Discussion

In this review, a literature survey of the PEM EL models, DC/DC converters suitable with PEM EL, and controller design of the hydrogen production system are carried out.

In the first step, different empirical and analytical modeling of PEM EL in the literature has been evaluated. There is only one static empirical model developed to describe the polarization curve [30,33–36]; this model is simple, considering the temperature and pressure effect, and it can predict the hydrogen production flow rate with a relative error of less than 2%. However, this modeling is only validated on the PEM EL single cell. Additionally, the activation overpotential and the concentration overpotential are not considered. This model still needs to be validated on many PEM EL stacks to evaluate their reliability and performance. Unlike static empirical models, few dynamic empirical PEM EL models are developed in the literature. The majority of these models are based on Randles circuits as shown in Figure 6 and the Randles–Warburg circuit as shown in Figure 7 [49–51,53,56]. Usually, the parameters of these models are derived using EIS or CI techniques, but these parameters remain valid around the operating point of PEM EL. Therefore, these identification techniques (EIS and CI) require an online implementation to make these models valid in a wide operating range, but this leads to an increase in the equipment cost added to implement this technique.

On the other hand, many semi-empirical models of PEM EL have been developed, and the static semi-empirical models describe the polarization curve V-I of PEM EL at steady-state and dynamic semi-empirical models that can be described as the dynamic behavior of PEM EL. These semi-empirical models are described by many equations based on physical and semi-empirical laws. These equations used to describe the physical phenomenon (reversible voltage, ohmic losses, activation losses, concentration losses, and double-layer charge capacitor) are summarized in Tables 1–8. The majority of these models are experimentally validated. Nevertheless, no study has been carried out to compare these different models to evaluate the performance and reliability of each model and select the appropriate models according to the targeted objective (diagnosis of PEM EL, efficiency control, hydrogen flow rate control, etc.).

The second step investigates the different sub-models that integrate with PEM EL models: firstly, a thermal sub-model that describes the stack temperature of PEM EL. Most thermal sub-models developed in the literature are based on the lumped thermal capacitance [4,59,62,67,99,107,110,111,127]. Contrary to fuel cells, many methods are adopted to describe the temperature in the PEM EL stack. Secondly, the efficiency of PEM EL (Faraday efficiency, voltage efficiency, and PEM EL efficiency) are investigated. In the literature, a few works considered this magnitude despite their importance in evaluating the PEM EL performances. Thirdly, regarding the gas flow rate produced and water consumed by PEM EL, Marangio [82] has developed a semi-empirical model that describes the different mass flow rates inside the cell. This issue has not been addressed in this review.

The third step aims to synthesize the current DC/DC converters used to supply the PEM EL in a DC bus configuration. Through the previous studies in the literature, it can be said that resonant IBC converters are good converters that can satisfy most of the requirements [145–150,152].

In the fourth step, a survey of the controllers used to control the hydrogen production system is based on the PEM EL. Most of the controllers are designed to control the DC/DC converter in order to ensure the global stability of the system (DC/DC converter-PEM EL), and other aims depend on the desired objective: regulation of the PEM EL voltage or PEM EL current to their references; control the hydrogen flow rate according to the state of charge of the hydrogen tanks and hydrogen consumed by fuel cells, and optimize the efficiency of PEM EL.

It can be observed that all proposed controllers (see Table 11) are based on the linearized model (static and dynamic), and most of them adopted the PI control. The nonlinear models should be checked and advanced control strategies for more reliability and validity need to be adopted.

The last step was regarding the PEM EL parameter identification issues. The PEM EL performance is very sensitive to parameter variation [6], so the identification parameters are crucial for a reliable and precise model. Many authors used offline identification [4,15,20,49,53,56,59,125]. However, the PEM EL can be operated in a wide operation range, especially when the PEM ELs are connected to the RES. For this reason, online identification remains the most efficient technique for accurate modeling of the controller performances and for a good diagnosis of PEM EL.

The analysis of PEM EL performance utilizing mathematical models has several limitations. Static models, which rely on empirical and semi-empirical approaches, may not fully capture the underlying physics of the system and are limited to describing the electrical characteristics at steady-state operation, neglecting dynamic behavior. The parameters used in these models are often obtained through experimental data, which can be difficult to obtain and may not be accurate or reliable. Furthermore, the models are often complex and challenging to interpret, making it difficult to diagnose issues or design controllers. Additionally, there is a lack of models that consider the effects of temperature and pressure on PEM EL performance, which are important factors in practical applications. Dynamic modeling of PEM EL is an area of ongoing research and development, with techniques such as EIS and CI not yet widely adopted and requiring specialized equipment.

The IBC topology is commonly used in PEM EL systems to convert DC power to a lower voltage. However, there are several limitations to this topology. Firstly, it may not be suitable for high voltage DC bus as it has a low voltage conversion ratio. Additionally, the IBC topology also has high voltage stress at the terminals of power switches. Furthermore, increasing the switching frequency in IBC improves the current ripple, power density, and dynamic performance, but it also increases the switching losses and the size and cost of additional passive components. These limitations should be considered when evaluating the performance and design of PEM electrolyzer systems that use the IBC topology.

The control strategy for the DC/DC converter-PEM EL system plays a crucial role in the efficient and effective operation of PEM EL. However, the specific goals of the controller vary depending on the type of hydrogen production configuration, such as PV-PEM EL or

wind turbine-PEM EL. One of the main objectives of the control strategy is to regulate the hydrogen flow rate through the PEM EL current, which is typically based on a constant reference, but this reference may vary depending on the operating conditions and the state of charge of the hydrogen tank. Regulating the PEM EL voltage to its reference voltage is another common control objective, but it can be challenging to maintain this reference voltage despite variations in the DC bus voltage and the operation point. A variety of control strategies, such as PI control, have been proposed in the literature, but they have limitations in terms of stability and robustness. Furthermore, the identification of PEM EL parameters, which is crucial for controller design, is often conducted offline, which can lead to less reliable and less accurate results due to the variability of the PEM EL parameters under different operating conditions. Therefore, it is important to consider these limitations when designing and implementing the control strategy for the DC/DC converter-PEM EL system.

8. Conclusions

Using an electrolyzer, storing electrical energy produced by RES in the form of hydrogen is one of the cleanest, most powerful, and promising energy storage methods. The PEM EL is one of the most commonly used types to produce hydrogen due to its reliability and efficiency compared to other types, such as alkaline and solid oxide electrolyzers. Several reviews have been reported in the literature about PEM EL modeling, as well as power converters suitable for use with PEM ELs. However, few studies have focused on controller design for the DC/DC converter-PEM EL system. Despite the importance of these three elements in providing a comprehensive and clear vision of the hydrogen production system based on PEM EL, no review has combined them. Therefore, this review presents various models of PEM ELs that are appropriate for use with DC/DC converters and discusses controller design. The second section presented the essential sub-models, such as the thermal sub-model to estimate the PEM EL temperature, the efficiency sub-model to evaluate the PEM EL efficiency, and the mass flow rate of gases necessary to estimate the hydrogen product. The third section investigated different DC/DC converters used to supply the PEM EL. Furthermore, this paper examined control laws that have been reported in the literature, as well as an identification technique used to estimate the parameters of the PEM EL.

Author Contributions: Conceptualization, M.K. and H.E.F.; methodology, M.K.; software, S.N. and T.B.; formal analysis, M.K. and Z.E.I.; investigation, A.R. and H.E.F.; resources, M.K.; data curation, M.K. and A.L.; writing—original draft preparation, M.K.; writing—review and editing, M.K.; visualization, M.K. and A.I.; supervision, H.E.F.; project administration, H.E.F.; All authors have read and agreed to the published version of the manuscript.

Funding: This research received no external funding.

Conflicts of Interest: We know of no conflicts of interest associated with this publication, and there has been no significant financial support for this work that could have influenced its outcome. As Corresponding Author, I confirm that the manuscript has been read and approved for submission by all the named authors.

Nomenclature

List of symbols and abbreviations

ARLS	Adaptative least square regression
CI	Current interruption
CTC	Charge transfer coefficient
DC/DC	Direct current/direct current
ECD	Exchange current density
EEC	Equivalent electrical circuit

EIS	Electrochemical impedance spectroscopy
EKF	Extended Kalman filter
GDL	Gas diffusion layer
IBC	Interleaved buck converter
IHBC	Isolated Half-Bridge Converter
KF	Kalman filter
LSR	Least square regression
MPC	Model predictive control
MPPT	Maximum power point tracker
NVR	Nature voltage response method
PEM EL	Proton exchange membrane electrolyzer
PI	Proportional integral
PID	Proportional-integral-derivative
PRBS	Pseudo-random binary sequence excitation
PSO	Particle swarm optimization
$D^w_{H^+}$	Concentration of protons participating in en masse diffusion
e	Parameterized pre-exponential factor of $i_{0,an}$
E_{act}	Activation energy required for the electron transport in the electrodes
E_{pro}	Activation energy required for the proton transport in the membrane
F	Faraday's constant
f	Parameterized coefficient of $i_{0,an}$
H_2	Hydrogen
H_2O	Water
H_2O_{con}	Water consumed by electrolysis process
I_{el}	Electrolyzer current
i	Current density
i_0	Electrode exchange current density
i_{Lim}	Diffusion limit current density
i_v	Current density of illumination
k	Constant parameter fitting
\dot{m}	Mass flow
N	Molar quantity of $O_2/H_2/H_2O$
\dot{N}	Molar flow rate of $O_2/H_2/H_2O$
N_{cell}	Number of cells
O_2	Oxygen
p	Pressure
P	Absorbed electrical power by PEM EL
P_{H_2}	Useful power of PEM EL
p_i	Partial pressure of the component i
$p^{sat}_{H_2O}$	Saturated water pressure
Q	Volumetric flow rate
\dot{Q}	Heat flow rate
R	Universal gas constant
$R(p,\theta)$	Equivalent resistance as a function of pressure Pa and temperature in C^0
$R(p,T)$	Equivalent resistance as a function of pressure in Pa and temperature in K
R_{th}	Thermal resistance
$s_1, s_2, s_3, r_1, r_2, t_1, t_2$ and t_3	Fitting parameters of Ullberg model
T	Temperature in Kelvin
T_m	Cooling medium temperature
v	Volume
V	Voltage
V_{HHV}	High heating value voltage of hydrogen
V_i	Ideal voltage of PEM electrolyzer
V_j	Drop voltage of j with $j = ohm/act/diff$
V_{log}	Logarithm voltage
V_{th}	Thermoneutral voltage
W_{e-heat}	Represents the electrical power dissipation as heat
z	Compressibility factor
Z_{wbg}	Warburg diffusion element
act	Activation

amb	Ambient
an/cat	Anode/cathode
cell	Cell
PV	Photovoltaic
RES	Renewable energy sources
SI	System identification
slpm	Standard liter per minute
SMC	Sliding mode control
WT	Wind turbine
A	Active surface area
a, b	Van der Waals coefficients
a_1, a_2, a_3, a_4 and a_5	Beattie–Bridgeman coefficients
$a_{R/P}$	Activity of reaction/product or water
B, C and D	Antoine coefficients
C_{dl}	Double-layer capacitance
C_{H^+}	Proton concentration
$C_{p\ H_2/O_2}$	Molar specific heat of H ₂ /O ₂
C_{th}	Lumped thermal capacity
C_x	Molar concentration of x species
$C_{H^+}^{\Sigma}$	Concentration of protons participating in surface diffusion
dR_{θ}	Ohmic resistance coefficient of temperature
$D_{H^+}^{\Sigma}$	Diffusion coefficient of protons for the surface diffusion mechanism
$D_{H^+}^G$	Diffusion coefficient of protons for the Grotthuss diffusion mechanism
cool	Cooling
diff	Diffusion
EL/el	Electrolyzer
ele	Electronic
env	Environment
eod	Electro-osmotic drag
gen	Generated
in	Input
init	Initial
loss	Losses
mem	Membrane
ohm	Ohmic
out	Output
pe	Pressure gradient
pump	Of the pump
ref	Reference condition
rev	Reversible voltage
stack	Of the stack
theo	Theoretical
ΔS_0	Entropy changes
ΔG_0	Gibbs' free energy change
ΔH_0	Enthalpy change
Δp	Differential pressure
Φ_{H_2/O_2}^{per}	Flux density across the membrane of H ₂ /O ₂
Φ	Parameter vectors
α	Charge transfer coefficient
δc	Stefan–Maxwell diffusion ratio
ε	Porosity of the membrane
μ	Concentration overpotential
ζ	Tortuosity factor
τ_{dl}	Time constant
θ	Temperature in degrees Celsius
δ	Membrane tackiness
σ	Membrane conductivity
ρ_{el}	Electronic conductor resistivity
λ	Membrane water content
κ	Experimental tuned coefficient

ℓ_{el}	Length of electronic conductors
η_{el}	Electrolyzer efficiency
γ	Roughness factor
η_F	Faraday efficiency
η_V	Voltage efficiency
η_{cell}	Cell efficiency
β	Experimentally defined coefficient

References

- Manzanedo, R.D.; Manning, P. COVID-19: Lessons for the climate change emergency. *Sci. Total Environ.* **2020**, *742*, 140563. [[CrossRef](#)]
- Jin, S. COVID-19, Climate Change, and Renewable Energy Research: We Are All in This Together, and the Time to Act Is Now. *ACS Energy Lett.* **2020**, *5*, 1709–1711. [[CrossRef](#)]
- Ngamroo, I. Robust coordinated control of electrolyzer and PSS for stabilization of microgrid based on PID-based mixed H₂/H_∞ control. *Renew. Energy* **2012**, *45*, 16–23. [[CrossRef](#)]
- Lebbal, M.E.; Lecœuche, S. Identification and monitoring of a PEM electrolyser based on dynamical modelling. *Int. J. Hydrog. Energy* **2009**, *34*, 5992–5999. [[CrossRef](#)]
- Rashid, M.M.; Mesfer, M.K.A.; Naseem, H.; Danish, M. Hydrogen Production by Water Electrolysis: A Review of Alkaline Water Electrolysis, PEM Water Electrolysis and High Temperature Water Electrolysis. *Int. J. Eng. Adv. Technol.* **2015**, *4*, 80–93.
- Toghyani, S.; Fakhradini, S.; Afshari, E.; Baniasadi, E.; Abdollahzadeh Jamalabadi, M.Y.; Safdari Shadloo, M. Optimization of operating parameters of a polymer exchange membrane electrolyzer. *Int. J. Hydrog. Energy* **2019**, *44*, 6403–6414. [[CrossRef](#)]
- Tijani, A.S.; Yusup, N.A.B.; Rahim, A.H.A. Mathematical Modelling and Simulation Analysis of Advanced Alkaline Electrolyzer System for Hydrogen Production. *Procedia Technol.* **2014**, *15*, 798–806. [[CrossRef](#)]
- Toshihiko, Y.; Koichi, K. Toyota MIRAI Fuel Cell Vehicle and Progress Toward a Future Hydrogen Society. *Electrochem. Soc. Interface* **2015**, *24*, 45.
- Grigoriev, S.A.; Kalinnikov, A.A. Mathematical modeling and experimental study of the performance of PEM water electrolysis cell with different loadings of platinum metals in electrocatalytic layers. *Int. J. Hydrog. Energy* **2017**, *42*, 1590–1597. [[CrossRef](#)]
- Pham, C.V.; Escalera-López, D.; Mayrhofer, K.; Cherevko, S.; Thiele, S. Essentials of High Performance Water Electrolyzers—From Catalyst Layer Materials to Electrode Engineering. *Adv. Energy Mater.* **2021**, *11*, 2101998. [[CrossRef](#)]
- Zhang, K.; Liang, X.; Wang, L.; Sun, K.; Wang, Y.; Xie, Z.; Wu, Q.; Bai, X.; Hamdy, M.S.; Chen, H.; et al. Status and perspectives of key materials for PEM electrolyzer. *Nano Res. Energy* **2022**, *1*, e9120032. [[CrossRef](#)]
- Jiang, G.; Yu, H.; Li, Y.; Yao, D.; Chi, J.; Sun, S.; Shao, Z. Low-Loading and Highly Stable Membrane Electrode Based on an Ir@WO(x)NR Ordered Array for PEM Water Electrolysis. *ACS Appl. Mater. Interfaces* **2021**, *13*, 15073–15082. [[CrossRef](#)] [[PubMed](#)]
- Onda, K.; Murakami, T.; Hikosaka, T.; Kobayashi, M.; Notu, R.; Ito, K. Performance Analysis of Polymer-Electrolyte Water Electrolysis Cell at a Small-Unit Test Cell and Performance Prediction of Large Stacked Cell. *J. Electrochem. Soc.* **2002**, *149*, A1069. [[CrossRef](#)]
- Hernández-Gómez, Á.; Ramirez, V.; Guilbert, D.; Saldívar, B. Development of an adaptive static-dynamic electrical model based on input electrical energy for PEM water electrolysis. *Int. J. Hydrog. Energy* **2020**, *45*, 18817–18830. [[CrossRef](#)]
- Guilbert, D.; Vitale, G. Dynamic Emulation of a PEM Electrolyzer by Time Constant Based Exponential Model. *Energies* **2019**, *12*, 750. [[CrossRef](#)]
- Guida, V.; Guilbert, D.; Douine, B. Candidate Interleaved DC-DC Buck Converters for Electrolyzers: State-of-the-Art and Perspectives. In Proceedings of the 2018 IEEE International Conference on Environment and Electrical Engineering and 2018 IEEE Industrial and Commercial Power Systems Europe, IEEEIC/I and CPS Europe 2018, Palermo, Italy, 12–15 June 2018.
- Guida, V.; Guilbert, D.; Douine, B. Literature Survey of Interleaved DC-DC StepDown Converters for Proton Exchange Membrane Electrolyzer Applications. *Trans. Environ. Electr. Eng.* **2019**, *3*, 33–43. [[CrossRef](#)]
- Yodwong, B.; Guilbert, D.; Phattanasak, M.; Kaewmanee, W.; Hinaje, M.; Vitale, G. AC-DC Converters for Electrolyzer Applications: State of the Art and Future Challenges. *Electronics* **2020**, *9*, 912. [[CrossRef](#)]
- Yodwong, B.; Guilbert, D.; Kaewmanee, W.; Phattanasak, M. Energy Efficiency Based Control Strategy of a Three-Level Interleaved DC-DC Buck Converter Supplying a Proton Exchange Membrane Electrolyzer. *Electronics* **2019**, *8*, 933. [[CrossRef](#)]
- Guilbert, D.; Yodwong, B.; Kaewmanee, W.; Phattanasak, M.; Hinaje, M. Hydrogen Flow Rate Control of a Proton Exchange Membrane Electrolyzer. In Proceedings of the 2019 Research, Invention, and Innovation Congress (RI2C), Bangkok, Thailand, 11–13 December 2019.
- Maamouri, R.; Guilbert, D.; Zasadzinski, M.; Rafaralahy, H. Proton exchange membrane water electrolysis: Modeling for hydrogen flow rate control. *Int. J. Hydrog. Energy* **2021**, *46*, 7676–7700. [[CrossRef](#)]
- Serna, Á.; Yahyaoui, I.; Normey-Rico, J.E.; de Prada, C.; Tadeo, F. Predictive control for hydrogen production by electrolysis in an offshore platform using renewable energies. *Int. J. Hydrog. Energy* **2017**, *42*, 12865–12876. [[CrossRef](#)]
- Rahim, A.A.; Tijani, A.S.; Kamarudin, S.; Hanapi, S. An overview of polymer electrolyte membrane electrolyzer for hydrogen production: Modeling and mass transport. *J. Power Sources* **2016**, *309*, 56–65. [[CrossRef](#)]

24. Olivier, P.; Bourasseau, C.; Bouamama, P.B. Low-temperature electrolysis system modelling: A review. *Renew. Sustain. Energy Rev.* **2017**, *78*, 280–300. [[CrossRef](#)]
25. Hernández-Gómez, Á.; Ramirez, V.; Guilbert, D. Investigation of PEM electrolyzer modeling: Electrical domain, efficiency, and specific energy consumption. *Int. J. Hydrog. Energy* **2020**, *45*, 14625–14639. [[CrossRef](#)]
26. Falcão, D.; Pinto, A. A review on PEM electrolyzer modelling: Guidelines for beginners. *J. Clean. Prod.* **2020**, *261*, 121184. [[CrossRef](#)]
27. Guilbert, D.; Collura, S.M.; Scipioni, A. DC/DC converter topologies for electrolyzers: State-of-the-art and remaining key issues. *Int. J. Hydrog. Energy* **2017**, *42*, 23966–23985. [[CrossRef](#)]
28. Yodwong, B.; Guilbert, D.; Phattanasak, M.; Kaewmanee, W.; Hinaje, M.; Vitale, G. Proton Exchange Membrane Electrolyzer Modeling for Power Electronics Control: A Short Review. *C—J. Carbon Res.* **2020**, *6*, 29. [[CrossRef](#)]
29. Folgado, F.J.; González, I.; Calderón, A.J. Simulation platform for the assessment of PEM electrolyzer models oriented to implement digital Replicas. *Energy Convers. Manag.* **2022**, *267*, 115917. [[CrossRef](#)]
30. Beainy, A.; Karami, N.; Moubayed, N. Simulink model for a PEM electrolyzer based on an equivalent electrical circuit. In Proceedings of the International Conference on Renewable Energies for Developing Countries 2014, Beirut, Lebanon, 26–27 November 2014.
31. Gorgun, H. Dynamic modelling of a proton exchange membrane (PEM) electrolyzer. *Int. J. Hydrog. Energy* **2006**, *31*, 29–38. [[CrossRef](#)]
32. Yigit, T.; Selamet, O.F. Mathematical modeling and dynamic Simulink simulation of high-pressure PEM electrolyzer system. *Int. J. Hydrog. Energy* **2016**, *41*, 13901–13914. [[CrossRef](#)]
33. Atlam, O. An experimental and modelling study of a photovoltaic/proton-exchange membrane electrolyser system. *Int. J. Hydrog. Energy* **2009**, *34*, 6589–6595. [[CrossRef](#)]
34. Atlam, O.; Kolhe, M. Equivalent electrical model for a proton exchange membrane (PEM) electrolyser. *Energy Convers. Manag.* **2011**, *52*, 2952–2957. [[CrossRef](#)]
35. Beainy, A.; Moubayed, N. Influence of variations of operating parameters on the functioning of a PEM electrolyzer and PEM fuel cell systems. In Proceedings of the 2016 Third International Conference on Electrical, Electronics, Computer Engineering and their Applications (EECEA), Beirut, Lebanon, 21–23 April 2016.
36. Albarghot, M.; Rolland, L. MATLAB/Simulink modelling and experimental results of a PEM electrolyzer powered by a solar panel. In Proceedings of the 2016 IEEE Electrical Power and Energy Conference (EPEC), Ottawa, ON, Canada, 12–14 October 2016.
37. Ulleberg, Ø. Modeling of advanced alkaline electrolyzers: A system simulation approach. *Int. J. Hydrog. Energy* **2003**, *28*, 21–33. [[CrossRef](#)]
38. Ulleberg, M. TRNSYS Simulation Models for Solar-Hydrogen Systems. *Sol. Energy* **1997**, *59*, 271–279. [[CrossRef](#)]
39. Zhou, T.; Francois, B. Modeling and control design of hydrogen production process for an active hydrogen/wind hybrid power system. *Int. J. Hydrog. Energy* **2009**, *34*, 21–30. [[CrossRef](#)]
40. Dieguez, P.; Ursua, A.; Sanchis, P.; Sopena, C.; Guelbenzu, E.; Gandia, L. Thermal performance of a commercial alkaline water electrolyzer: Experimental study and mathematical modeling. *Int. J. Hydrog. Energy* **2008**, *33*, 7338–7354. [[CrossRef](#)]
41. Deshmukh, S.S.; Boehm, R.F. Review of modeling details related to renewably powered hydrogen systems. *Renew. Sustain. Energy Rev.* **2008**, *12*, 2301–2330. [[CrossRef](#)]
42. Ziogou, C.; Ipsakis, D.; Seferlis, P.; Bezergianni, S.; Papadopoulou, S.; Voutetakis, S. Optimal production of renewable hydrogen based on an efficient energy management strategy. *Energy* **2013**, *55*, 58–67. [[CrossRef](#)]
43. Liso, V.; Savoia, G.; Araya, S.S.; Cinti, G.; Kær, S.K. Modelling and Experimental Analysis of a Polymer Electrolyte Membrane Water Electrolysis Cell at Different Operating Temperatures. *Energies* **2018**, *11*, 3273. [[CrossRef](#)]
44. Rakousky, C.; Reimer, U.; Wippermann, K.; Carmo, M.; Lueke, W.; Stolten, D. An analysis of degradation phenomena in polymer electrolyte membrane water electrolysis. *J. Power Sources* **2016**, *326*, 120–128. [[CrossRef](#)]
45. Rakousky, C.; Reimer, U.; Wippermann, K.; Kuhri, S.; Carmo, M.; Lueke, W.; Stolten, D. Polymer electrolyte membrane water electrolysis: Restraining degradation in the presence of fluctuating power. *J. Power Sources* **2017**, *342*, 38–47. [[CrossRef](#)]
46. Siracusano, S.; Trocino, S.; Briguglio, N.; Baglio, V.; Arico, A.S. Electrochemical Impedance Spectroscopy as a Diagnostic Tool in Polymer Electrolyte Membrane Electrolysis. *Materials* **2018**, *11*, 1368. [[CrossRef](#)]
47. Li, N.; Araya, S.S.; Kær, S.K. Long-term contamination effect of iron ions on cell performance degradation of proton exchange membrane water electrolyser. *J. Power Sources* **2019**, *434*, 226755. [[CrossRef](#)]
48. Wang, H.; Gaillard, A.; Hissel, D. Online electrochemical impedance spectroscopy detection integrated with step-up converter for fuel cell electric vehicle. *Int. J. Hydrog. Energy* **2019**, *44*, 1110–1121. [[CrossRef](#)]
49. Ganeshan, I.S.; Manikandan, V.V.S.; Ram Sundhar, V.; Sajiv, R.; Shanthi, C.; Kottayil, S.K.; Ramachandran, T. Regulated hydrogen production using solar powered electrolyser. *Int. J. Hydrog. Energy* **2016**, *41*, 10322–10326. [[CrossRef](#)]
50. van der Merwe, J.; Uren, K.; van Schoor, G.; Bessarabov, D. Characterisation tools development for PEM electrolyzers. *Int. J. Hydrog. Energy* **2014**, *39*, 14212–14221. [[CrossRef](#)]
51. Martinson, C.A.; Schoor, G.V.; Uren, K.; Bessarabov, D.; Merwe, J.H.P.V.D. Characterisation of a Proton Exchange Membrane Electrolyser Using Electrochemical Impedance Spectroscopy. Ph.D. Thesis, North-West University, Potchefstroom, South Africa, 2012.

52. Rezaei Niya, S.M.; Hoorfar, M. Study of proton exchange membrane fuel cells using electrochemical impedance spectroscopy technique—A review. *J. Power Sources* **2013**, *240*, 281–293. [[CrossRef](#)]
53. Martinson, C.; Van Schoor, G.; Uren, K.; Bessarabov, D. Equivalent electrical circuit modelling of a Proton Exchange Membrane electrolyser based on current interruption. In Proceedings of the 2013 IEEE International Conference on Industrial Technology (ICIT), Cape Town, South Africa, 25–28 February 2013.
54. Zhang, L.; Zhou, Z.; Chen, Q.; Long, R.; Quan, S. Model Predictive Control for Electrochemical Impedance Spectroscopy Measurement of Fuel Cells Based on Neural Network Optimization. *IEEE Trans. Transp. Electrification* **2019**, *5*, 524–534. [[CrossRef](#)]
55. Hong, P.; Li, J.; Xu, L.; Ouyang, M.; Fang, C. Modeling and simulation of parallel DC/DC converters for online AC impedance estimation of PEM fuel cell stack. *Int. J. Hydrog. Energy* **2016**, *41*, 3004–3014. [[CrossRef](#)]
56. Martinson, C.A.; van Schoor, G.; Uren, K.R.; Bessarabov, D. Characterisation of a PEM electrolyser using the current interrupt method. *Int. J. Hydrog. Energy* **2014**, *39*, 20865–20878. [[CrossRef](#)]
57. Biaku, C.; Dale, N.; Mann, M.; Salehfar, H.; Peters, A.; Han, T. A semiempirical study of the temperature dependence of the anode charge transfer coefficient of a 6kW PEM electrolyzer. *Int. J. Hydrog. Energy* **2008**, *33*, 4247–4254. [[CrossRef](#)]
58. Dale, N.V.; Mann, M.D.; Salehfar, H. Semiempirical model based on thermodynamic principles for determining 6kW proton exchange membrane electrolyzer stack characteristics. *J. Power Sources* **2008**, *185*, 1348–1353. [[CrossRef](#)]
59. Espinosa-López, M.; Darras, C.; Poggi, P.; Glises, R.; Baucour, P.; Rakotondrainibe, A.; Besse, S.; Serre-Combe, P. Modelling and experimental validation of a 46 kW PEM high pressure water electrolyzer. *Renew. Energy* **2018**, *119*, 160–173. [[CrossRef](#)]
60. Ma, Z.; Witteman, L.; Wrubel, J.A.; Bender, G. A comprehensive modeling method for proton exchange membrane electrolyzer development. *Int. J. Hydrog. Energy* **2021**, *46*, 17627–17643. [[CrossRef](#)]
61. Zhang, Z.; Xing, X. Simulation and experiment of heat and mass transfer in a proton exchange membrane electrolysis cell. *Int. J. Hydrog. Energy* **2020**, *45*, 20184–20193. [[CrossRef](#)]
62. Aouali, F.Z.; Becherif, M.; Tabanjat, A.; Emziane, M.; Mohammedi, K.; Krehi, S.; Khellaf, A. Modelling and Experimental Analysis of a PEM Electrolyser Powered by a Solar Photovoltaic Panel. *Energy Procedia* **2014**, *62*, 714–722. [[CrossRef](#)]
63. Ayivor, P.; Torres, J.; Van Der Meijden, M.A.M.M.; Van Der Pluijm, R.; Stouwie, B. Modelling of Large Size Electrolyzer for Electrical Grid Stability Studies in Real Time Digital Simulation. In Proceedings of the 3rd International Hybrid Power Systems Workshop, Tenerife, Spain, 8–9 May 2018.
64. Selamet, Ö.F.; Becerikli, F.; Mat, M.D.; Kaplan, Y. Development and testing of a highly efficient proton exchange membrane (PEM) electrolyzer stack. *Int. J. Hydrog. Energy* **2011**, *36*, 11480–11487. [[CrossRef](#)]
65. Ursua, A.; Gandia, L.M.; Sanchis, P. Hydrogen Production From Water Electrolysis: Current Status and Future Trends. *Proc. IEEE* **2012**, *100*, 410–426. [[CrossRef](#)]
66. LeRoy, R.L. The Thermodynamics of Aqueous Water Electrolysis. *J. Electrochem. Soc.* **1980**, *127*, 1954. [[CrossRef](#)]
67. Webster, J.; Bode, C. Implementation of a Non-Discretized Multiphysics PEM Electrolyzer Model in Modelica. In Proceedings of the 13th International Modelica Conference, Regensburg, Germany, 4–6 March 2019; pp. 833–840.
68. Laoun, B. Thermodynamics aspect of high pressure hydrogen production by water electrolysis. *Rev. Energ. Renouvelables* **2007**, *10*, 435–444.
69. Olivier, P.; Bourasseau, C.; Bouamama, B. Dynamic and multiphysic PEM electrolysis system modelling: A bond graph approach. *Int. J. Hydrog. Energy* **2017**, *42*, 14872–14904. [[CrossRef](#)]
70. Millet, P. Water Electrolysis for Hydrogen Generation. *Electrochem. Technol. Energy Storage Convers.* **2012**, *2*, 383–423.
71. García-Valverde, R.; Espinosa, N.; Urbina, A. Optimized method for photovoltaic-water electrolyser direct coupling. *Int. J. Hydrog. Energy* **2011**, *36*, 10574–10586. [[CrossRef](#)]
72. Dedigama, I.; Angeli, P.; Ayers, K.; Robinson, J.B.; Shearing, P.R.; Tsaoulidis, D.; Brett, D.J.L. In situ diagnostic techniques for characterisation of polymer electrolyte membrane water electrolyzers—Flow visualisation and electrochemical impedance spectroscopy. *Int. J. Hydrog. Energy* **2014**, *39*, 4468–4482. [[CrossRef](#)]
73. Moradi Nafchi, F.; Baniasadi, E.; Afshari, E.; Javani, N. Performance assessment of a solar hydrogen and electricity production plant using high temperature PEM electrolyzer and energy storage. *Int. J. Hydrog. Energy* **2018**, *43*, 5820–5831. [[CrossRef](#)]
74. Lopes, C.; Watanabe, E.H. Experimental and theoretical development of a pem electrolyzer model applied to energy storage systems. In Proceedings of the 2009 Brazilian Power Electronics Conference, Bonito-Mato Grosso do Sul, Brazil, 27 September–1 October 2009; pp. 775–782.
75. Awasthi, A.; Scott, K.; Basu, S. Dynamic modeling and simulation of a proton exchange membrane electrolyzer for hydrogen production. *Int. J. Hydrog. Energy* **2011**, *36*, 14779–14786. [[CrossRef](#)]
76. Han, B.; Steen, S.M.; Mo, J.; Zhang, F.Y. Electrochemical performance modeling of a proton exchange membrane electrolyzer cell for hydrogen energy. *Int. J. Hydrog. Energy* **2015**, *40*, 7006–7016. [[CrossRef](#)]
77. Koponen, J.; Kosonen, A.; Ruuskanen, V.; Huoman, K.; Niemelä, M.; Ahola, J. Control and energy efficiency of PEM water electrolyzers in renewable energy systems. *Int. J. Hydrog. Energy* **2017**, *42*, 29648–29660. [[CrossRef](#)]
78. Ruuskanen, V.; Koponen, J.; Huoman, K.; Kosonen, A.; Niemelä, M.; Ahola, J. PEM water electrolyzer model for a power-hardware-in-loop simulator. *Int. J. Hydrog. Energy* **2017**, *42*, 10775–10784. [[CrossRef](#)]
79. Nie, J.; Chen, Y.; Boehm, R.F.; Katukota, S. A Photoelectrochemical Model of Proton Exchange Water Electrolysis for Hydrogen Production. *J. Heat Transf.* **2008**, *130*, 042409. [[CrossRef](#)]

80. Moradi Nafchi, F.; Afshari, E.; Baniasadi, E.; Javani, N. A parametric study of polymer membrane electrolyser performance, energy and exergy analyses. *Int. J. Hydrog. Energy* **2019**, *44*, 18662–18670. [[CrossRef](#)]
81. Abdin, Z.; Webb, C.J.; Gray, E.M. Modelling and simulation of a proton exchange membrane (PEM) electrolyser cell. *Int. J. Hydrog. Energy* **2015**, *40*, 13243–13257. [[CrossRef](#)]
82. Marangio, F.; Santarelli, M.; Cali, M. Theoretical model and experimental analysis of a high pressure PEM water electrolyser for hydrogen production. *Int. J. Hydrog. Energy* **2009**, *34*, 1143–1158. [[CrossRef](#)]
83. Chase, M.W., Jr.; Davies, C.A.; Downey, J.R. *JANAF Thermochemical Tables*; American Institute of Physics: New York, NY, USA, 1985.
84. Rozain, C.; Millet, P. Electrochemical characterization of Polymer Electrolyte Membrane Water Electrolysis Cells. *Electrochim. Acta* **2014**, *131*, 160–167. [[CrossRef](#)]
85. Suermann, M.; Pătru, A.; Schmidt, T.J.; Büchi, F.N. High pressure polymer electrolyte water electrolysis: Test bench development and electrochemical analysis. *Int. J. Hydrog. Energy* **2017**, *42*, 12076–12086. [[CrossRef](#)]
86. Kim, H.; Park, M.; Lee, K.S. One-dimensional dynamic modeling of a high-pressure water electrolysis system for hydrogen production. *Int. J. Hydrog. Energy* **2013**, *38*, 2596–2609. [[CrossRef](#)]
87. Tijani, A.S.; Haiyoon, M.A. Simulation Analysis of the Effect of Temperature and Exchange Current Density on Power and Hydrogen Production of (PEM) Electrolyzer. *Appl. Mech. Mater.* **2014**, *660*, 411–415. [[CrossRef](#)]
88. Chandesris, M.; Médeau, V.; Guillet, N.; Chelghoum, S.; Thoby, D.; Fouda-Onana, F. Membrane degradation in PEM water electrolyzer: Numerical modeling and experimental evidence of the influence of temperature and current density. *Int. J. Hydrog. Energy* **2014**, *40*, 1353–1366. [[CrossRef](#)]
89. Colbertaldo, P.; Gómez Aláez, S.L.; Campanari, S. Zero-dimensional dynamic modeling of PEM electrolyzers. *Energy Procedia* **2017**, *142*, 1468–1473. [[CrossRef](#)]
90. Fragiacomio, P.; Genovese, M. Modeling and energy demand analysis of a scalable green hydrogen production system. *Int. J. Hydrog. Energy* **2019**, *44*, 30237–30255. [[CrossRef](#)]
91. Maroufmashat, A.; Seyyedyn, F.; Roshandel, R.; Bouroshaki, M. Hydrogen generation optimization in a hybrid photovoltaic-electrolyzer using intelligent techniques. In Proceedings of the ASME 2012 10th International Conference on Fuel Cell Science, Engineering and Technology Collocated with the ASME 2012 6th International Conference on Energy Sustainability, San Diego, CA, USA, 23–26 July 2012.
92. Nation, D.D.; Smith, K.L. Modelling the Dynamics of a Polymer Electrolyte Membrane (PEM) Electrolyser at Start-Up. *Caribb. Ann.* **2016**, *1*–23.
93. Sayedin, F.; Maroufmashat, A.; Roshandel, R.; Khavas, S.S. Optimal design and operation of a photovoltaic–electrolyser system using particle swarm optimisation. *Int. J. Sustain. Energy* **2014**, *35*, 566–582. [[CrossRef](#)]
94. Dedigama, I.; Ayers, K.; Shearing, P.R.; Brett, D.J. An experimentally validated steady state polymer electrolyte membrane water electrolyser model. *Int. J. Electrochem. Sci.* **2014**, *9*, 2662–2681.
95. Nieminen, J.; Dincer, I.; Naterer, G. Comparative performance analysis of PEM and solid oxide steam electrolyzers. *Int. J. Hydrog. Energy* **2010**, *35*, 10842–10850. [[CrossRef](#)]
96. Zhang, X.; Zeng, R.; Du, T.; He, Y.; Tian, H.; Mu, K.; Liu, X.; Li, H. Conventional and energy level based exergoeconomic analysis of biomass and natural gas fired polygeneration system integrated with ground source heat pump and PEM electrolyzer. *Energy Convers. Manag.* **2019**, *195*, 313–327. [[CrossRef](#)]
97. Ogumerem, G.S.; Pistikopoulos, E.N. Parametric optimization and control for a smart Proton Exchange Membrane Water Electrolysis (PEMWE) system. *J. Process Control* **2020**, *91*, 37–49. [[CrossRef](#)]
98. Aubras, F.; Deseure, J.; Kadjo, J.J.A.; Dedigama, I.; Majasan, J.; Grondin-Perez, B.; Chabriat, J.P.; Brett, D.J.L. Two-dimensional model of low-pressure PEM electrolyser: Two-phase flow regime, electrochemical modelling and experimental validation. *Int. J. Hydrog. Energy* **2017**, *42*, 26203–26216. [[CrossRef](#)]
99. Aouali, F.Z.; Becherif, M.; Ramadan, H.S.; Emziane, M.; Khellaf, A.; Mohammedi, K. Analytical modelling and experimental validation of proton exchange membrane electrolyser for hydrogen production. *Int. J. Hydrog. Energy* **2017**, *42*, 1366–1374. [[CrossRef](#)]
100. Carmo, M.; Fritz, D.L.; Mergel, J.; Stolten, D. A comprehensive review on PEM water electrolysis. *Int. J. Hydrog. Energy* **2013**, *38*, 4901–4934. [[CrossRef](#)]
101. Ojong, E.T.; Kwan, J.T.H.; Nouri-Khorasani, A.; Bonakdarpour, A.; Wilkinson, D.P.; Smolinka, T. Development of an experimentally validated semi-empirical fully-coupled performance model of a PEM electrolysis cell with a 3-D structured porous transport layer. *Int. J. Hydrog. Energy* **2017**, *42*, 25831–25847. [[CrossRef](#)]
102. Khalid, F.; Bicer, Y. High temperature electrolysis of hydrogen bromide gas for hydrogen production using solid oxide membrane electrolyzer. *Int. J. Hydrog. Energy* **2020**, *45*, 5629–5635. [[CrossRef](#)]
103. Choi, P.; Jalani, N.H.; Datta, R. Thermodynamics and proton transport in nafion: II. Proton diffusion mechanisms and conductivity. *J. Electrochem. Soc.* **2005**, *152*, E123. [[CrossRef](#)]
104. Choi, P. A simple model for solid polymer electrolyte (SPE) water electrolysis. *Solid State Ion.* **2004**, *175*, 535–539. [[CrossRef](#)]
105. Agbli, K.S.; Péra, M.C.; Hissel, D.; Rallières, O.; Turpin, C.; Doumbia, I. Multiphysics simulation of a PEM electrolyser: Energetic Macroscopic Representation approach. *Int. J. Hydrog. Energy* **2011**, *36*, 1382–1398. [[CrossRef](#)]
106. Lee, B.; Park, K.; Kim, H.-M. Dynamic Simulation of PEM Water Electrolysis and Comparison with Experiments. *Int. J. Electrochem. Sci.* **2013**, *8*, 235–248.

107. Trifkovic, M.; Sheikhzadeh, M.; Nigim, K.; Daoutidis, P. Modeling and Control of a Renewable Hybrid Energy System With Hydrogen Storage. *IEEE Trans. Control Syst. Technol.* **2014**, *22*, 169–179. [[CrossRef](#)]
108. Sartory, M.; Wallnöfer-Ogris, E.; Salman, P.; Fellingner, T.; Justl, M.; Trattner, A.; Klell, M. Theoretical and experimental analysis of an asymmetric high pressure PEM water electrolyser up to 155 bar. *Int. J. Hydrog. Energy* **2017**, *42*, 30493–30508. [[CrossRef](#)]
109. Tijani, A.S.; Ghani, M.F.A.; Rahim, A.H.A.; Muritala, I.K.; Binti Mazlan, F.A. Electrochemical characteristics of (PEM) electrolyzer under influence of charge transfer coefficient. *Int. J. Hydrog. Energy* **2019**, *44*, 27177–27189. [[CrossRef](#)]
110. García-Valverde, R.; Espinosa, N.; Urbina, A. Simple PEM water electrolyser model and experimental validation. *Int. J. Hydrog. Energy* **2011**, *37*, 1927–1938. [[CrossRef](#)]
111. Sharifian, S.; Asasian Kolar, N.; Harasek, M. Transient simulation and modeling of photovoltaic-PEM water electrolysis. *Energy Sources Part A Recovery Util. Environ. Eff.* **2019**, *42*, 1097–1107. [[CrossRef](#)]
112. Ruuskanen, V.; Koponen, J.; Kosonen, A.; Hehemann, M.; Keller, R.; Niemelä, M.; Ahola, J. Power quality estimation of water electrolyzers based on current and voltage measurements. *J. Power Sources* **2020**, *450*, 227603. [[CrossRef](#)]
113. Zhang, H.; Lin, G.; Chen, J. Evaluation and calculation on the efficiency of a water electrolysis system for hydrogen production. *Int. J. Hydrog. Energy* **2010**, *35*, 10851–10858. [[CrossRef](#)]
114. Harrison, K.W.; Hernández-Pacheco, E.; Mann, M.; Salehfar, H. Semiempirical Model for Determining PEM Electrolyzer Stack Characteristics. *J. Fuel Cell Sci. Technol.* **2006**, *3*, 220–223. [[CrossRef](#)]
115. Ni, M.; Leung, M.K.H.; Leung, D.Y.C. Energy and exergy analysis of hydrogen production by a proton exchange membrane (PEM) electrolyzer plant. *Energy Convers. Manag.* **2008**, *49*, 2748–2756. [[CrossRef](#)]
116. Fontes, G. Modelisation et Caracterisation de la pile PEM Pour l'Etude des Interactions Avec les Convertisseurs Statiques. Ph.D. Thesis, Laboratoire d'Electrotechnique et d'Electronique, l'institut national polytechnique de Toulouse, Toulouse, France, 2005.
117. Dahbi, S.; Aboutni, R.; Aziz, A.; Benazzi, N.; Elhafyani, M.; Kassmi, K. Optimised hydrogen production by a photovoltaic-electrolysis system DC/DC converter and water flow controller. *Int. J. Hydrog. Energy* **2016**, *41*, 20858–20866. [[CrossRef](#)]
118. Mohamed, B.; Alli, B.; Ahmed, B. Using the hydrogen for sustainable energy storage: Designs, modeling, identification and simulation membrane behavior in PEM system electrolyser. *J. Energy Storage* **2016**, *7*, 270–285. [[CrossRef](#)]
119. Guilbert, D.; Sorbera, D.; Vitale, G. A stacked interleaved DC-DC buck converter for proton exchange membrane electrolyzer applications: Design and experimental validation. *Int. J. Hydrog. Energy* **2020**, *45*, 64–79. [[CrossRef](#)]
120. Harvey, R.; Abouatallah, R.; Cargnelli, J. *PEM Electrolysis for Hydrogen Production: Principles and Applications*; CRC press: Boca Raton, FL, USA, 2016.
121. Dhirde, A.M.; Dale, N.V.; Salehfar, H.; Mann, M.D.; Han, T.-H. Equivalent Electric Circuit Modeling and Performance Analysis of a PEM Fuel Cell Stack Using Impedance Spectroscopy. *IEEE Trans. Energy Convers.* **2010**, *25*, 778–786. [[CrossRef](#)]
122. Larminie, J.; Dicks, A. *Fuel Cell Systems Explained*, 2nd ed.; J. Wiley: Chichester, UK, 2003.
123. Nehrir, M.H.; Wang, C. *Modeling and Control of Fuel Cells*; John Wiley & Sons: Hoboken, NJ, USA, 2009.
124. Wang, C.; Nehrir, M.H.; Shaw, S.R. Dynamic models and model validation for PEM fuel cells using electrical circuits. *IEEE Trans. Energy Convers.* **2005**, *20*, 442–451. [[CrossRef](#)]
125. Guilbert, D.; Vitale, G. Experimental Validation of an Equivalent Dynamic Electrical Model for a Proton Exchange Membrane Electrolyzer. In Proceedings of the 2018 IEEE International Conference on Environment and Electrical Engineering and 2018 IEEE Industrial and Commercial Power Systems Europe, IEEEIC/I and CPS Europe 2018, Palermo, Italy, 12–15 June 2018; pp. 1–6.
126. Lee, C.-Y.; Chen, C.-H.; Li, S.-C.; Wang, Y.-S. Development and application of flexible integrated microsensor as real-time monitoring tool in proton exchange membrane water electrolyzer. *Renew. Energy* **2019**, *143*, 906–914. [[CrossRef](#)]
127. Mori, M.; Mržljak, T.; Drobnič, B.; Sekavčnik, M. Integral Characteristics of Hydrogen Production in Alkaline Electrolysers. *Stroj. Vestn.—J. Mech. Eng.* **2013**, *10*, 585–594. [[CrossRef](#)]
128. Ghribi, D.; Khelifa, A.; Diaf, S.; Belhamel, M. Study of hydrogen production system by using PV solar energy and PEM electrolyser in Algeria. *Int. J. Hydrog. Energy* **2012**, *38*, 8480–8490. [[CrossRef](#)]
129. Barbir, F. PEM electrolysis for production of hydrogen from renewable energy sources. *Sol. Energy* **2005**, *78*, 661–669. [[CrossRef](#)]
130. Becker, S.; Karri, V. Predictive models for PEM-electrolyzer performance using adaptive neuro-fuzzy inference systems. *Int. J. Hydrog. Energy* **2010**, *35*, 9963–9972. [[CrossRef](#)]
131. Schalenbach, M.; Carmo, M.; Fritz, D.L.; Mergel, J.; Stolten, D. Pressurized PEM water electrolysis: Efficiency and gas crossover. *Int. J. Hydrog. Energy* **2013**, *38*, 14921–14933. [[CrossRef](#)]
132. Al-refai, M.A. Matlab/Simulink Simulation of Solar Energy Storage System. *Int. J. Electr. Comput. Energetic Electron. Commun. Eng.* **2014**, *8*, 304–309.
133. Sarrias-Mena, R.; Fernández-Ramírez, L.M.; García-Vázquez, C.A.; Jurado, F. Electrolyzer models for hydrogen production from wind energy systems. *Int. J. Hydrog. Energy* **2015**, *40*, 2927–2938. [[CrossRef](#)]
134. Konstantinopoulos, S.A.; Anastasiadis, A.G.; Vokas, G.A.; Kondylis, G.P.; Polyzakis, A. Optimal management of hydrogen storage in stochastic smart microgrid operation. *Int. J. Hydrog. Energy* **2018**, *43*, 490–499. [[CrossRef](#)]
135. Hassan, A.H.; Liao, Z.; Wang, K.; Abdelsamie, M.M.; Xu, C.; Wang, Y. Exergy and Exergoeconomic Analysis for the Proton Exchange Membrane Water Electrolysis under Various Operating Conditions and Design Parameters. *Energies* **2022**, *15*, 8247. [[CrossRef](#)]
136. Wang, Z.; Wang, X.; Chen, Z.; Liao, Z.; Xu, C.; Du, X. Energy and exergy analysis of a proton exchange membrane water electrolysis system without additional internal cooling. *Renew. Energy* **2021**, *180*, 1333–1343. [[CrossRef](#)]

137. Olivier, P.; Bourasseau, C.; Bouamama, B. Modelling, simulation and analysis of a PEM electrolysis system. *IFAC-PapersOnLine* **2016**, *49*, 1014–1019. [[CrossRef](#)]
138. Millet, P.; Mbemba, N.; Grigoriev, S.A.; Fateev, V.N.; Aukauloo, A.; Etiévant, C. Electrochemical performances of PEM water electrolysis cells and perspectives. *Int. J. Hydrog. Energy* **2011**, *36*, 4134–4142. [[CrossRef](#)]
139. Caisheng, W. Modeling And Control Of Hybrid Wind Photovoltaic/Fuel Cell Distributed Generation Systems. Ph.D. Thesis, Montana State University, Bozeman, MT, USA, 2006.
140. Cavallaro, C.; Cecconi, V.; Chimento, F.; Musumeci, S.; Santonocito, C.; Sapuppo, C. Bridge Converter for the Energy Management of Electrolyzer Systems. In Proceedings of the 2007 IEEE International Symposium on Industrial Electronics, Vigo, Spain, 4–7 June 2007.
141. Blinov, A.; Andrijanovits, A. New DC/DC Converter for Electrolyser Interfacing with Stand-Alone Renewable Energy System. *Electr. Control Commun. Eng.* **2012**, *1*, 24–29. [[CrossRef](#)]
142. Gautam, D.S.; Bhat, A.K.S. A Comparison of Soft-Switched DC-to-DC Converters for Electrolyzer Application. *IEEE Trans. Power Electron.* **2013**, *28*, 54–63. [[CrossRef](#)]
143. Şahin, M.E.; Okumuş, H.İ.; Aydemir, M.T. Implementation of an electrolysis system with DC/DC synchronous buck converter. *Int. J. Hydrog. Energy* **2014**, *39*, 6802–6812. [[CrossRef](#)]
144. Lee, I.-O.; Cho, S.-Y.; Moon, G.-W. Interleaved Buck Converter Having Low Switching Losses and Improved Step-Down Conversion Ratio. *IEEE Trans. Power Electron.* **2012**, *27*, 3664–3675. [[CrossRef](#)]
145. Tsai, C.-T.; Shen, C.-L. Interleaved soft-switching buck converter with coupled inductors. In Proceedings of the 2008 IEEE International Conference on Sustainable Energy Technologies, Singapore, 24–27 November 2008.
146. Premalatha, R.; Murugesan, P. Soft switching model of Interleaved Buck converter. *J. Theor. Appl. Inf. Technol.* **2015**, *74*, 131–134.
147. Cha, D.-J.; Baek, J.-E.; Cho, Y.-M.; Ko, K.-C.; Lee, W.-C. Development of interleaved buck converter using soft-switching for high current applications. In Proceedings of the 2014 IEEE International Power Modulator and High Voltage Conference (IPMHVC), Santa Fe, NM, USA, 1–5 June 2014.
148. Ilic, M.; Maksimovic, D. Interleaved Zero-Current-Transition Buck Converter. *IEEE Trans. Ind. Appl.* **2007**, *43*, 1619–1627. [[CrossRef](#)]
149. Esteki, M.; Adib, E.; Farzanehfard, H. Soft switching interleaved PWM buck converter with one auxiliary switch. In Proceedings of the 2014 22nd Iranian Conference on Electrical Engineering (ICEE), Tehran, Iran, 20–22 May 2014.
150. Esteki, M.; Poorali, B.; Adib, E.; Farzanehfard, H. High step-down interleaved buck converter with low voltage stress. *IET Power Electron.* **2015**, *8*, 2352–2360. [[CrossRef](#)]
151. Esteki, M.; Poorali, B.; Adib, E.; Farzanehfard, H. Interleaved Buck Converter With Continuous Input Current, Extremely Low Output Current Ripple, Low Switching Losses, and Improved Step-Down Conversion Ratio. *IEEE Trans. Ind. Electron.* **2015**, *62*, 4769–4776. [[CrossRef](#)]
152. Chandrasekhar, P.; Reddy, S.R. Performance of soft-switched DC-DC resonant converter for Electrolyzer. In Proceedings of the 2011 4th International Symposium on Resilient Control Systems, Boise, ID, USA, 9–11 August 2011.
153. Ingole, D.; Drgoňa, J.; Kalúz, M.; Klaučo, M.; Bakošová, M.; Kvasnica, M. Model predictive control of a combined electrolyzer-fuel cell educational pilot plant. In Proceedings of the 2017 21st International Conference on Process Control (PC), Strbske Pleso, Slovakia, 6–9 June 2017.
154. Torok, L.; Mathe, L.; Nielsen, C.K.; Munk-Nielsen, S. Modeling and Control of Three-Phase Grid-Connected Power Supply With a Small DC-Link Capacitor for Electrolyzers. *IEEE Trans. Ind. Appl.* **2017**, *53*, 4634–4643. [[CrossRef](#)]
155. Koundi, M.; El Fadil, H.; Rachid, A.; El Idrissi, Z.; Giri, F.; Guerrero, J. Output Feedback Sliding Mode Control of PEM EL-IBC System for Hydrogen Production. *IFAC-PapersOnLine* **2019**, *52*, 85–90. [[CrossRef](#)]
156. Koundi, M.; El Fadil, H. Mathematical modeling of PEM electrolyzer and design of a voltage controller by the SMPWM approach. In Proceedings of the 2019 International Conference on Power Generation Systems and Renewable Energy Technologies (PGSRET), Istanbul, Turkey, 26–27 August 2019.
157. Török, L.; Nielsen, C.K.; Munk-Nielsen, S.; Rømer, C.; Flindt, P. High efficiency electrolyser power supply for household hydrogen production and storage systems. In Proceedings of the 2015 17th European Conference on Power Electronics and Applications (EPE'15 ECCE-Europe), Geneva, Switzerland, 8–10 September 2015.
158. Collura, S.M.; Guilbert, D.; Vitale, G.; Luna, M.; Alonge, F.; D'Ippolito, F.; Scipioni, A. Design and experimental validation of a high voltage ratio DC/DC converter for proton exchange membrane electrolyzer applications. *Int. J. Hydrog. Energy* **2019**, *44*, 7059–7072. [[CrossRef](#)]
159. Nafeh, A.E.-S.A. Hydrogen production from a PV/PEM electrolyzer system using a neural-network-based MPPT algorithm. *Int. J. Numer. Model. Electron. Netw. Devices Fields* **2011**, *24*, 282–297. [[CrossRef](#)]
160. Koundi, M.; El Idrissi, Z.; El Fadil, H.; Belhaj, F.Z.; Lassoui, A.; Gaouzi, K.; Rachid, A.; Giri, F. State-Feedback Control of Interleaved Buck-Boost DC-DC Power Converter with Continuous Input Current for Fuel Cell Energy Sources: Theoretical Design and Experimental Validation. *World Electr. Veh. J.* **2022**, *13*, 124. [[CrossRef](#)]
161. Ettihir, K.; Boulon, L.; Becherif, M.; Agbossou, K.; Ramadan, H.S. Online identification of semi-empirical model parameters for PEMFCs. *Int. J. Hydrog. Energy* **2014**, *39*, 21165–21176. [[CrossRef](#)]

162. Guilbert, D.; Vitale, G. Variable parameters model of a PEM electrolyzer based model reference adaptive system approach. In Proceedings of the 2020 IEEE International Conference on Environment and Electrical Engineering and 2020 IEEE Industrial and Commercial Power Systems Europe (EEEIC/I&CPS Europe), Madrid, Spain, 9–12 June 2020.
163. Hernández-Gómez, A.; Ramirez, V.; Guilbert, D.; Saldivar, B. Cell voltage static-dynamic modeling of a PEM electrolyzer based on adaptive parameters: Development and experimental validation. *Renew. Energy* **2021**, *163*, 1508–1522. [[CrossRef](#)]

Disclaimer/Publisher's Note: The statements, opinions and data contained in all publications are solely those of the individual author(s) and contributor(s) and not of MDPI and/or the editor(s). MDPI and/or the editor(s) disclaim responsibility for any injury to people or property resulting from any ideas, methods, instructions or products referred to in the content.